

NIST Spectroscopy Beamline Suite: Soft and Tender X-ray Spectroscopy and Microscopy (SST)

Contents

	Acronyms.....	3
	Abstract.....	4
	Introduction	5
	Axes Definition	6
1	Scientific Programs and Technical Scope	7
	1.1 Accelerating Organic Photovoltaics with Soft and Tender Spectroscopy and Microscopy	8
	1.2 Nanoscale Spectroscopy for Next Generation Semiconductor Microelectronics: CMOS and Beyond.....	11
	1.3 Technical Scope.....	15
	1.4 Development and Advisory Team	16
2	SST beamline.....	18
	2.1 Source	18
	2.2 Front End	24
	Figure 2.9: Parameters and FEA result for the SST front-end fixed aperture mask.2.3 White Beam Section	26
	2.4 Beamline Optics	33
	2.5 Radiation Shielding.....	52
3	Endstations	60
	3.1 Discussion of endstations	60

	3.2	Beamline Utilities	65
	3.3	Equipment Protection System and Personnel Protection System	65
	3.4	Laboratory Space and Access.....	69
	3.5	Work Area	69
4		Major Technical Risk Items	70
	4.1	Complexity of the beamlines	70
	4.2	Relocation/Re-use of endstations	70
	4.3	Operating hutch-less up to 7.5 keV.....	70
	4.4	Repurposed Undulators from ESRF and Wisconsin.....	70
	4.5	Endstation Issues	70
5		Safety.....	72

Acronyms

BDP	Beamline Development Proposal
CM	Collimating Mirror
DCM	Double-Crystal Monochromator
DW	Damping Wiggler
FE	Front End
FMK	Fixed Aperture Mask
FOE	First Optical Enclosure
FXI	Full-Field X-ray Imaging
HXN	Hard X-ray Nanoprobe
ISS	Inner Shell Spectroscopy
NEXAFS	Near Edge X-ray Absorption Fine Structure
SRX	Submicron Resolution X-ray Spectroscopy
SSA	Secondary Source Aperture
TM	Toroidal Mirror
XANES	X-ray Absorption Near Edge Structure
XPD	X-ray Powder Diffraction
XPS	X-ray Photoelectron Spectroscopy
XBPM	X-ray Beam Position Monitor "X"

Abstract

SST beamline is one of the two NIST spectroscopy suites of state-of-the-art high throughput beamlines at the NSLS-II. The scientific case and capability of SST is described in the beamline development proposal (BDP): Soft and Tender X-ray Spectroscopy and Microscopy (100 eV to 7.5 keV canted sources). This final design report (FDR) describes the following topics:

- Brief summary of the scientific case.
- The design of the beamline in terms of the source (two canted out-of-vacuum undulators).
- The optical design (two branches for soft and tender x-rays respectively, with the rare capability that two endstations on the tender branch can also receive beam from the soft branch.
- Discussion of end stations that are to be transferred from the NSLS to SST beamline.
- Analysis on radiation shielding design including that of Bremsstrahlung, secondary Bremsstrahlung and synchrotron x rays.
- Analysis on thermal management of the white-beam components; and analysis of technical and schedule risks.

Introduction

The National Institute of Standards and Technology (NIST) and the Department of Energy (DOE) have a 30 year ongoing partnership at the NSLS and NSLS-II developing advanced synchrotron measurement methods and delivering excellence in material science impacting important societal challenges in energy, health, environment, national security, and improving our quality of life. This partnership promotes innovation and enhances US industrial competitiveness for inorganic and organic semiconductors, photovoltaics, self-assembled-monolayers, biological and environmental materials, batteries, catalysts, fuel cells, polymers, superconductors, ferroelectrics, and ferromagnets. Located at the NSLS, the NIST Synchrotron Methods Group of nine staff have operated a suite of three state-of-the-art spectroscopy beamlines (U7A, X24A, and X23A2) that span the entire absorption-edge energy range of the periodic table to establish structure function relationships in advanced materials. More than 200 industry and academic researchers each year have used the NIST Beamline Suite to accelerate the development of new materials into devices and systems with advanced functionality for a broad spectrum of industries. Building upon this success, NIST is currently in the process of establishing an NSLS-II spectroscopy suite of two state-of-the-art high throughput beamlines (with X-ray Diffraction capability) described in beamline development proposals; *Soft and Tender X-ray Spectroscopy and Microscopy (100 eV to 7.5 keV canted sources)* and *Hard X-ray Absorption Spectroscopy and Diffraction (4.5 keV to 22 keV three-pole wiggler source)*. Taken together, the NIST NSLS-II Spectroscopy Beamline Suite will be capable of measuring the electronic, chemical, and structural properties of almost any material, often at the nanoscale. NIST is committed to fully funding the construction of its proposed Spectroscopy Beamline Suite and to continuous world leading improvements in synchrotron measurement science and technology. Furthermore, NIST will build upon its NSLS based Synchrotron Science Group to fully staff its stakeholder relationship in NSLS-II.

Axes Definition

Unless otherwise specified, the axes definition used in this document is shown in Figure 1. X rays travel in the positive Z direction and X is the horizontal direction where positive is away from the storage ring. The vertical axis is Y, where up is positive. Rotations are referred according to the rotation axis.

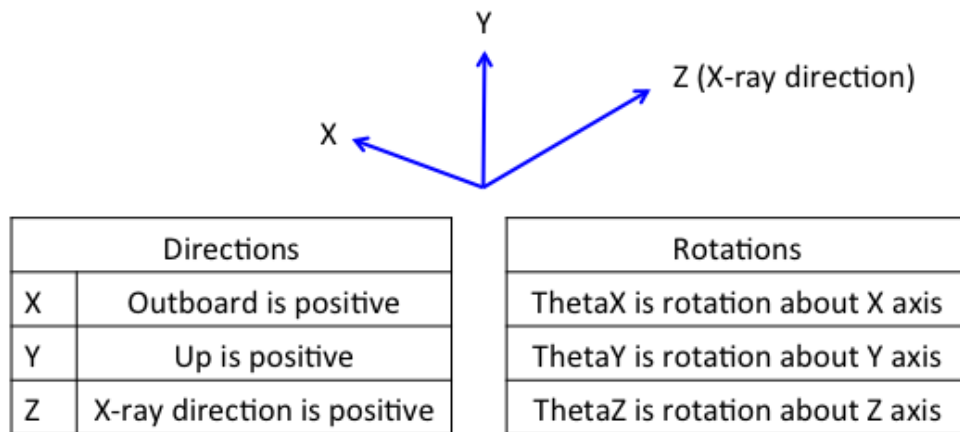


Figure 1: Axes definition used in this PDR. X-rays travel in the positive Z direction.

1 Scientific Programs and Technical Scope

Synchrotron based X-ray Photoelectron Spectroscopy (XPS) and Near Edge X-ray Absorption Fine Structure (NEXAFS) spectroscopies are complementary techniques, probing occupied and unoccupied density of states respectively. The ability to perform both measurements on the same sample achieves a complete, non-destructive, depth selective measurement of electronic structure, chemistry, and bond orientation.

NIST proposes to build a pair of spectroscopy beamlines based on two canted undulator sources, one for soft x rays (100 eV to 2.2 keV) and one for tender x rays (1 keV to 7.5 keV). The beamlines will have a total of 6 unique world class NEXAFS/XPS experimental stations (2 full-field microscopes, 2 automated high-throughput, and 2 *in-situ* high pressure); four will be served by the soft x-ray undulator and two by the tender x-ray undulator, thus a variety of soft and tender spectroscopy experiments can be accomplished simultaneously in this beamline complex. Two of the experimental stations (high-throughput XPS/NEXAFS and the XPS microscope) can utilize the soft and tender x-ray undulators (sequentially or even simultaneously) enabling a continuous selection of x-rays from 100 eV to 7.5 keV (at a common focal point) in a single experiment to enhance depth selectivity in XPS; i.e. in Hard X-ray Photoelectron Spectroscopy - HAXPES which will be the only undulator-based HAXPES facility in the U.S.A.

Enabled by the world class brightness of the NIST NSLS-II canted undulator beamline pair, NIST has pioneered (at NSLS) two new and unique (large depth of field for practical materials) magnetic projection microscopes pushing the state-of-the-art in synchrotron XPS and NEXAFS spectroscopy full field imaging measurement science. The XPS microscope combines nanometer scale spatial resolution with chemical and electronic state specificity and full three-dimensional mapping of the structure of nanomaterials and nanodevices at all points within their volume. The large area imaging NEXAFS microscope will produce highly efficient, highly parallel spectroscopic chemical and orientation maps of gradient samples, combinatorial arrays (e.g. 1000s of compositional samples at a time), and device arrays up to 4 cm² with simultaneous micron scale resolution.

The proposed Soft and Tender X-ray Spectroscopy and Microscopy (SST) beamline pair coupled with NIST's continuous development of automated high-throughput spectroscopy methods, world class high efficiency detectors, and unique NEXAFS and XPS microscopes will have a large scale impact on the materials science of important societal challenges in energy, health, environment, and national security.

In sections 1.1 and 1.2, we highlight areas of scientific interest for the SST beamlines with two examples:

- 1) Accelerating Organic Photovoltaics with Soft and Tender Spectroscopy and Microscopy.
- 2) Nanoscale Spectroscopy for Next Generation Semiconductor Microelectronics: CMOS and Beyond.

These cases demonstrate the types of research that would be uniquely served by the SST beamline. They illustrate how this proposed beamline pair will establish structure function relationships in advanced materials, often at the nanoscale, to accelerate the development of new materials into devices and systems with advanced functionality for promoting innovation and enhancing US industrial competitiveness.

Ten additional diverse science case examples are included in NSLS-II Beamline Development Proposal: NIST Spectroscopy Beamline Suite: Soft and Tender X-ray Spectroscopy and Microscopy (SST), pages 14-45, that discuss the following topics:

- 3) Designing Biomaterials with High Through-Put Screening: Using the NIST NEXAFS Microscope
- 4) Synchrotron Spectroscopy an Enabling Capability for the Defense and National Security Community
- 5) Nano to Microscale Spectroscopy for Environmentally Friendly Marine Anti-Fouling Coatings
- 6) Spectroscopy and Microscopy for Advanced Hard and Soft Materials: Energy and Microelectronics
- 7) Advanced Spectroscopy Promoting Breakthrough Catalysis for Energy Applications

The BDP for SST beamline is included in Appendix F.

1.1 Accelerating Organic Photovoltaics with Soft and Tender Spectroscopy and Microscopy

Affordable, renewable power generation, a critical component of U.S. energy independence, has remained for many years perpetually on the threshold of technical and economic viability. The largest solar power development efforts have focused on incremental improvements of older technologies, and even with these efforts, photovoltaics still produce less than 0.7 % of our national electrical energy needs.

New solar energy technologies, such as organic photovoltaics (OPV), promise to break this paradigm by greatly reducing both the manufacturing costs and the capital required to increase production (Fig.1.1a). The active layers of an OPV module are formulated as liquid inks that can be applied to flexible surfaces using simple graphics arts printing techniques such as inkjet, spray, and screen printing, to create solar cell modules that can be spread over large areas as easily as

unrolling a carpet. The commercialization of OPV technology has been slowed by two key technical challenges: enhancing the power conversion efficiency, and preventing aging-related performance loss. To address these challenges requires precise measurements of materials composition and molecular orientation with sub-100 nm spatial resolution. These needs will be met by SST to greatly accelerate the development of high-efficiency, long-lasting solar modules with the potential to build a new domestic solar cell manufacturing industry in the U.S. and transform our energy production landscape in the coming decades.

The power conversion efficiency of bulk heterojunction (BHJ) OPV devices critically depends on the distribution of the polymer absorber and the fullerene electron acceptor (e.g., the blend morphology). Synchrotron-based tools provide a critical means to probe the structure of the BHJ layer, shown in Fig.1.1b. For example, NIST recently applied Near-Edge X-ray Absorption Fine Structure (NEXAFS) spectroscopy to reveal that the vertical distribution of BHJ components follows segregation behavior similar to that of miscible polymer blends. The top (air) interface becomes rich in the polymer absorber, whereas the bottom interface depends on the substrate. This effect greatly impacts charge carrier mobility measurement; transistors fabricated from BHJs can exhibit ambipolar or hole-only transport depending on the dielectric. These results were extended to practical photovoltaic devices by comparing BHJs cast upon hole transport layers that have similar work functions but different surface energies. The molecular orientation of the absorber revealed by NEXAFS contributed to the development of accurate optical models for the practical devices. This work illustrates the importance of non-destructive interface measurements via high-throughput, automated NEXAFS to the acceleration of OPV technology development. High-throughput, automated NEXAFS acquisition on 100s of PV samples is required to rapidly build structure function relationships for intelligent PV materials design and processing.

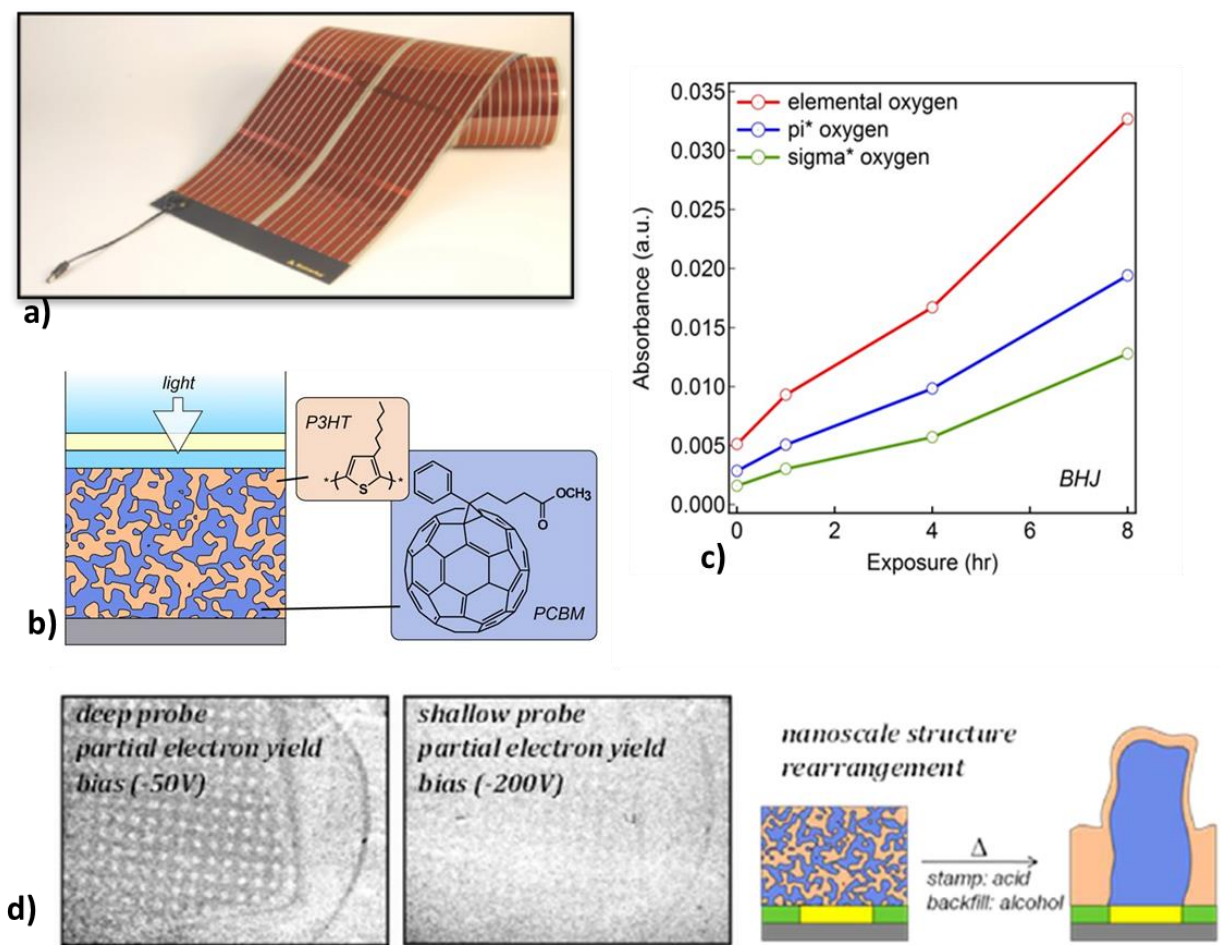


Figure 1.1: a) Picture showing Konarka's Power Plastic organic[®] organic photovoltaics module. NIST has an active CRADA with Konarka (Lowell, MA). b) The BHJ active-layer morphology is critical to its power conversion efficiency. c) NEXAFS measurement of oxygen incorporation into an OPV active layer. d) NIST's NEXAFS microscope(NSLS U7A) reveals the structure of an OPV film structured "by design" in collaboration with University of Washington (Ginger). Lighter areas are fullerene-rich; contrast is generated by split π^* resonance of fullerene.

The ideal OPV system has a three-dimensional domain network structure with dimensions less than 100 nm. Small changes to the distributions of domain size and shape strongly impact OPV performance. Composition-sensitive microscopy methods with high spatial resolution are thus critical to the measurement and rapid optimization of OPV active layer structure. To this end, NIST recently demonstrated a new, full-field NEXAFS microscope at U7A beamline that is capable of measuring the three-dimensional compositional structure of OPV films. The images in Fig.1.1d show a BHJ film "by design" that has been purposefully structured by thermal annealing atop a chemically patterned template. The fullerene component is attracted to the high energy acid surface (yellow), whereas the polymer absorber is attracted to the lower energy alcohol surface (green). The powerful depth resolution of NEXAFS microscopy is revealed by comparing images

collected at shallow and deep bias conditions. The loss of contrast at the shallow condition reveals that the surface is covered with a ~ 2 nm thick “skin” of the polymer. This information is required to understand and eventually control the three-dimensional domain structure of OPV active layers. Although compelling, the images are proofs-of-concept with a ≈ 300 μm diameter stamp; the sub-micron resolutions of the proposed Larger Area Imaging NEXAFS Microscope and XPS (3D-Chemical) Microscope at SST are required to approach lateral resolutions that are relevant to the frontiers of OPV technology. Whereas the XPS microscope will provide the most powerful measurement of domain structure, the NEXAFS microscope will be required to determine how variations in composition are correlated to variations in local orientation, which is critical to local photon absorption and nanoscale exciton / charge carrier transport processes.

NEXAFS and XPS microscopy will also impact OPV technology development in the measurement of aging-related performance loss. High vertical and lateral resolutions are required to determine the precise locations of chemical degradation products. The unique 100 eV to 7.5 keV energy range of the SST beamlines will provide unprecedented depth selectivity to measure the vertical distribution of degradation products near interfaces. Recent NEXAFS measurements, shown in Fig.1.1c, at U7A beamline have shown the technique to be quite sensitive to oxygen incorporation in OPV materials. The polymer absorber is found to be chemically vulnerable at the point where a side chain is added to enhance solubility and aid processing. Oxygen π^* and σ^* resonance intensities increase commensurately, indicating a carboxyl-containing oxidation product. By nondestructively identifying the mechanisms of degradation, and their location within devices, these tools will greatly accelerate the development and deployment of robust, high-efficiency plastic solar cells.

1.2 Nanoscale Spectroscopy for Next Generation Semiconductor Microelectronics: CMOS and Beyond

SEMATECH is a non-profit consortium established more than 20 years ago to perform basic research in semiconductor manufacturing. In recent years, the consortium of leading semiconductor manufacturers has set global direction and bridged strategic R&D to manufacturing with a business model based on highly flexible collaboration and demonstrated internal information control.

Today, SEMATECH continues accelerating the next technology revolution with nanoelectronics and emerging technology partners including federally funded research initiatives that directly enhance applications in information technology, communications, medicine, energy, and national security. SEMATECH has engaged in collaboration with the NIST Synchrotron Methods Group stationed at the NSLS and during the past 6 years has conducted state of the art research at each of NIST’s three

NSLS spectroscopy beamlines for materials screening and optimization research: X23A2, X24A, and U7A for EXAFS, high-energy XPS, and NEXAFS. Two current examples of DARPA funded SEMATECH programs include: i) Sub-threshold-slope Transistors for Electronics with Extremely-low Power (STEEP) and ii) Carbon Electronics for RF Applications (CERA).

The STEEP program goal is to develop a revolutionary transistor technology for logic circuits with extremely low power consumption while maintaining high performance for logic applications in areas such as unattended sensors with unlimited lifetimes or autonomous unmanned air vehicles navigated by vision systems. The key technical challenges of achieving steep-sub threshold-slopes over many decades of current; developing novel circuit designs accommodating asymmetric source-drain regions; demonstrating abrupt doping profiles at tunneling junctions; and integrating SiGe, Ge, or III-V compound semiconductors in transistor structures to facilitate the required tunneling currents – all require the most advanced analytical tools equipped with the highest spatial resolution available to assure success. SEMATECH is extremely excited anticipating process optimization results from samples studied via the new NIST NSLS-II soft and tender beamline pair for NEXAFS, high energy XPS, and chemical imaging. These new capabilities will uniquely impact the STEEP and other SEMATECH programs by enabling simultaneous nanoscale spatial resolution and depth selectivity (via variable kinetic energy high-energy XPS in the range of 100 eV to 7.5 keV) essentially operating as a rapid, non-destructive 3D XPS microscope at the nanoscale.

The CERA program targets development of wafer-scale graphene synthesis focused on enabling ultra-high-speed, low-power graphene-channel field-effect transistors through innovative approaches that enable revolutionary advances in materials science, epitaxial growth, transistor development, and RF circuit design. The research needed to achieve the goals of the CERA program is another area where NIST's proposed advanced synchrotron spectroscopy imaging techniques and advanced measurement instruments are pivotal to success. An example of the critical need for high-throughput low energy polarized NEXAFS as a probe for characterizing the electronic structure of graphene has recently been demonstrated in University of Buffalo-SEMATECH-NIST collaboration on NIST beamline U7A at the NSLS, which resulted in a publication on Cu/graphene substrate hybridization. Figure 1.2 illustrates the best resolved splitting (reported in the literature) of the π^* absorption feature and indisputable evidence for the existence of an interlayer state that has been the subject of sharp debate for more than 20 years. These exciting results have stimulated the collaborative interest of theorists and modeling and simulation of the NEXAFS spectra is in progress.

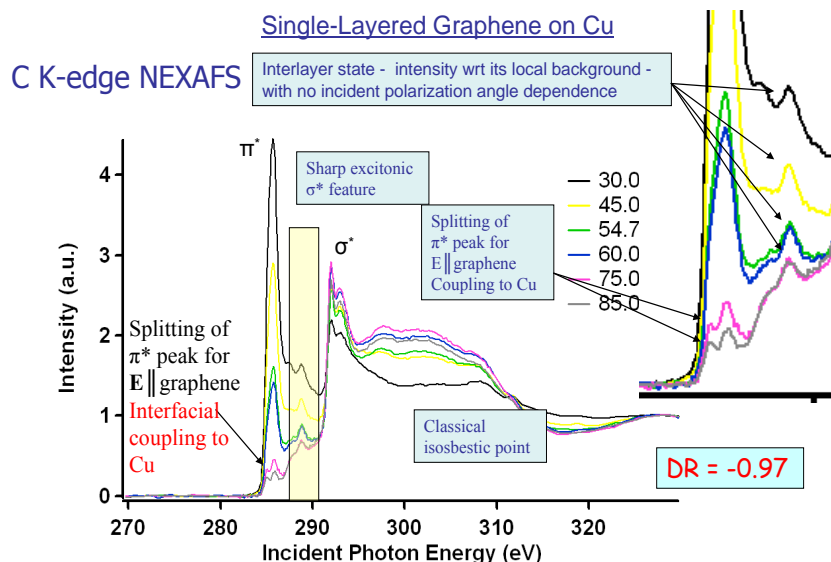


Figure 1.2: Polarization dependent NEXAFS spectra of single layer graphene on Cu foil which illustrates evidence of π^* splitting (at high polarization angles) and the interlayer state (inset).

In addition to the STEEP and CERA programs, all of the planar and non-planar CMOS logic and non-volatile memory device programs at SEMATECH are materials limited and critical challenges associated with continued device scaling have demonstrated a clear and urgent need for both of NIST's proposed microscopes (nano and micro scales).

For example, there is a universal need to identify surface chemical states as a function of processing as achieved recently with NEXAFS measurements at NIST beamline U7A ($\text{HfO}_2/\text{Al}_2\text{O}_3$, probing the outermost 1 nm of material as shown in Fig.1.3a).

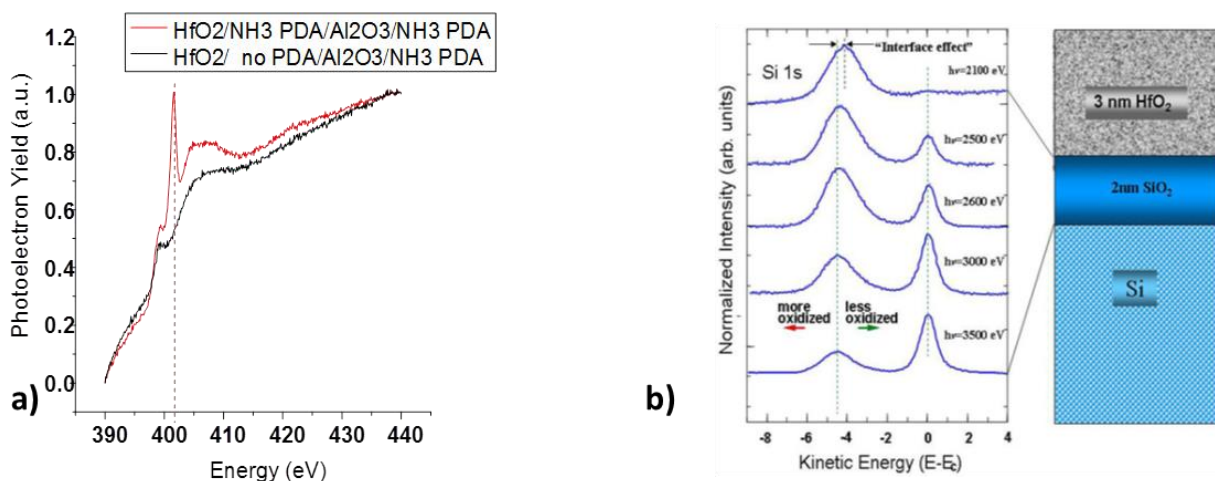


Figure 1.3: a) Surface sensitive N K edge absorption spectra shows that Al in-diffusion into HfO_2 (black curve) is limited when HfO_2 is preannealed in NH_3 ambient, evident by surface Al-N peak (red). b) Si 1s spectra from 3nm HfO_2 / 2nm SiO_2 sample recorded with variable kinetic energy high-energy XPS (VKE-XPS) illustrates depth profiling and an interface effect near HfO_2 / SiO_2 interface.

Also to determine the corresponding changes in binding energies of chemical constituents of buried layers and interfaces as measured with tender XPS on NIST beamline X24A (HfO_2 / SiO_2 , shown in Fig.1.3b) and detecting variations in oxidation state of underlying engineered substrate elements (SiGe, shown in Fig. 1.4), in order to ultimately explain the mechanisms that give rise to the limits of electrical performance. All these examples have a common need for spectroscopy of large numbers of samples generated by numerous materials and processing parameters, SST beamlines with their high-throughput NEXAFS/XPS stations will fully answer this challenge.

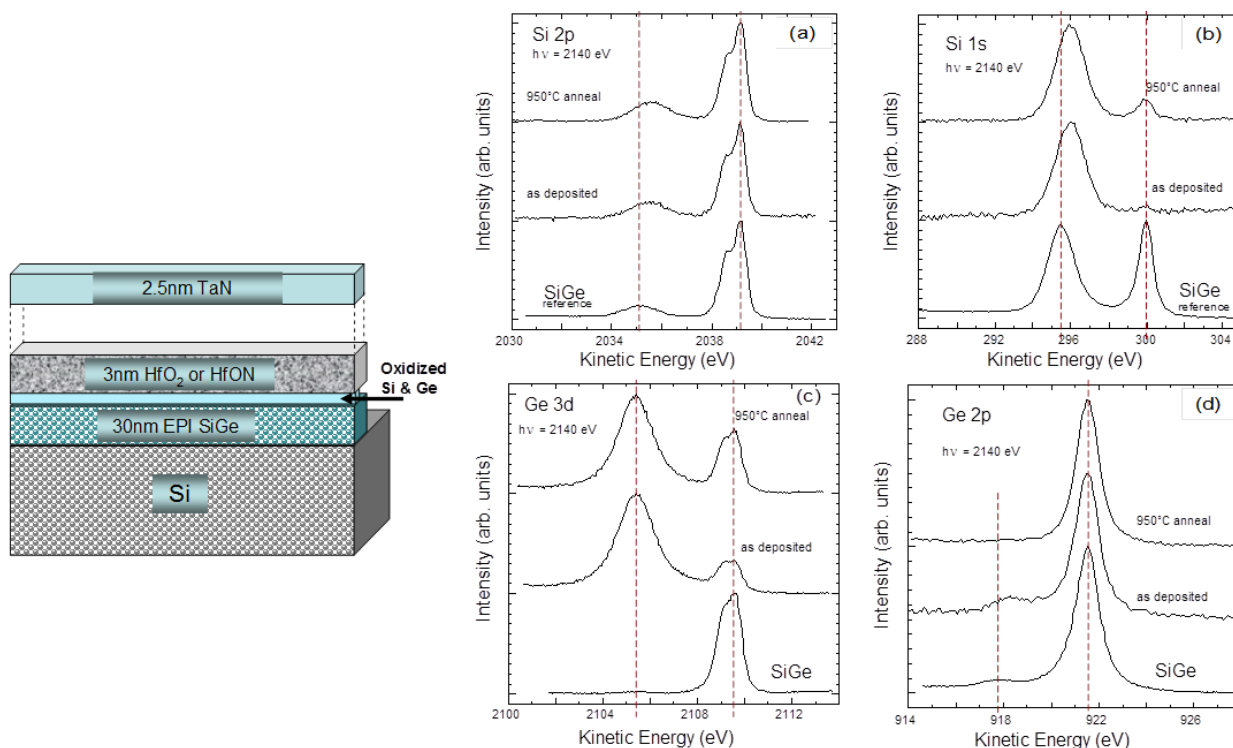


Figure 1.4: Material stack measured by high-energy XPS (a-d) on NIST beamline X24A at the NSLS. Acquisition of bulk sensitive (Si 2p, Ge 3d) and surface sensitive (Si 1s, Ge 2p) core lines allows the oxidation kinetics as a function of processing to be determined.

An example of the diverse and challenging device architectures and novel film systems verses power that are slated for manufacturing on a timeline according to *The International Technology Roadmap for Semiconductors 2009 edition* are given in Fig.1.5.

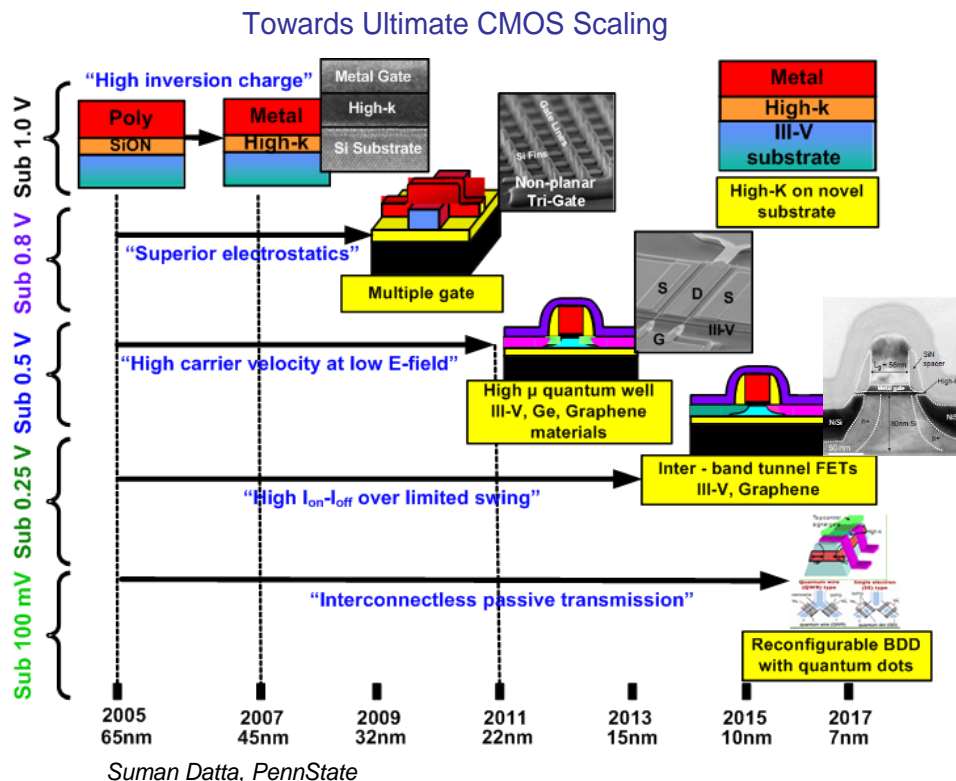


Figure 1.5: CMOS scaling time-line predicted by Suman Datta, PennState.

These architectures are currently being researched (many with no known solution). The proposed NIST XPS microscope with nano-scale spatial resolution is ideally suited to the timeline construction and materials (65 nm down to 7 nm resolution).

1.3 Technical Scope

The SST’s pair of spectroscopy beamlines are served by two insertion devices symmetrically canted at an angle of 2 mrad: a 0.84 m long EPU device for < 100-2200 eV (soft x-rays) and a 1.6 m U-42 undulator covering the range 1.5-7.5 keV (tender x-rays). The newly developed full-field XPS microscope requires a spot size of 10 microns over the full energy range of both beamlines that mandates locating the insertion devices at a low beta straight section of NSLS-II. The undulator sources deliver adequate brightness and flux for the microscopes, high resolution XPS, soft x-ray fluorescence yield NEXAFS and emission spectroscopy, and high-throughput (>10 times NSLS) electron yield NEXAFS.

The soft x-ray beamline is based on a variable line spacing plane grating monochromator (VLSPGM) capable of delivering a resolving power higher than 20,000 over its full energy range. The tender x-ray beamline is based on an extended range (theta: -3 degrees to 85 degrees) double-crystal monochromator (LN₂ cooled DCM) equipped with interchangeable YB66, Si(111), and Si(220) crystals to achieve medium and high resolution (Si(333) reflection near normal incidence). The expected flux in all experimental stations of the beamline pair will be in the range 10^{12} - 10^{13} photons/s with resolving powers between a few thousands and 10^4 .

The beamline pair will have 6 unique world-class NEXAFS/XPS experimental stations as shown schematically in Fig.1.6. The automated high-throughput HAXPES/XPS/NEXAFS station and XPS/HAXPES microscope utilize both monochromatic soft and tender beams enabling a continuous selection of x rays from 100 eV to 7.5 keV at a common focal point in a single experiment. Computer controlled mirrors and pass-through beams are used to rapidly switch soft and tender x rays between the 6 stations to fully utilize and optimize all the available beamtime (an extension of NIST's NSLS U7A beamline operation among 4 endstations). The high-energy limit (7.5 keV) was chosen so that the two beamlines could operate with the various end stations directly on the experimental floor; i.e., without experimental hutches.

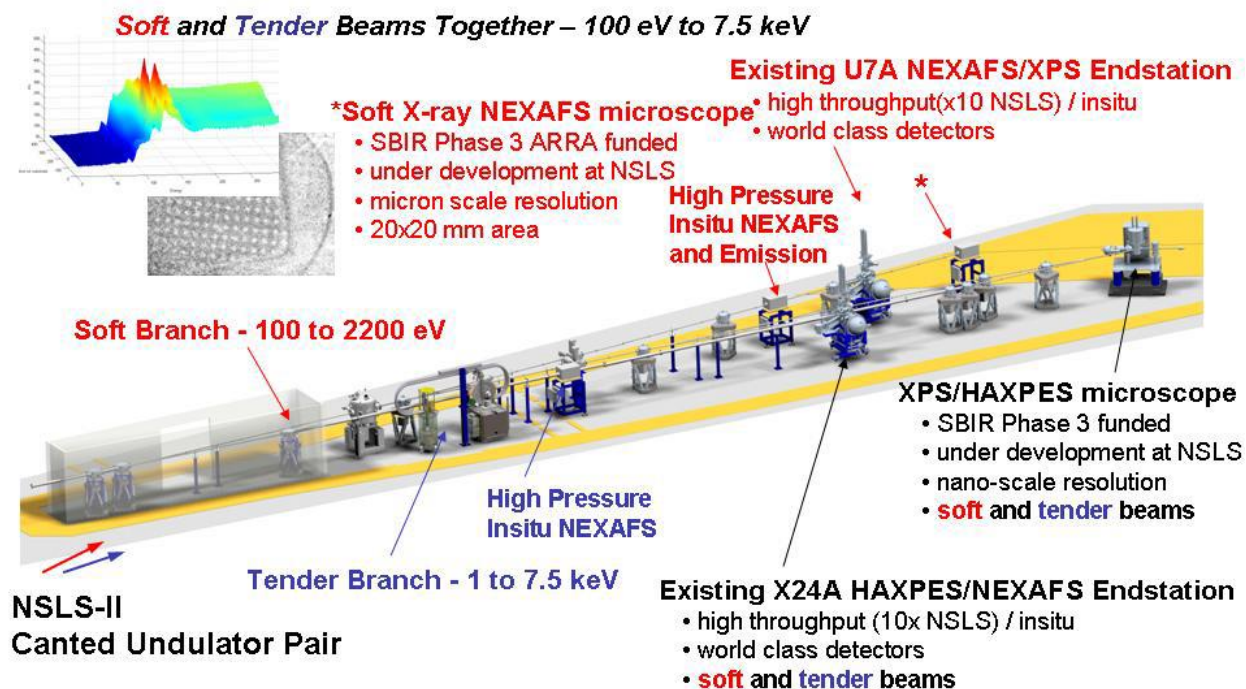


Figure 1.6: Arrangement of the 6 world-class NEXAFS/XPS experimental stations at the SST beamline.

1.4 Development and Advisory Team

The development team consists of NIST team led by Dan Fischer, and BNL team led by Andrew Broadbent. The team includes Ruben Reininger, Ray Browning, Zugen Fu, Barry Karlin, Conan Weiland, Johnny Kirkland, Eliot Gann, Nick Quackenbush, Chernojaye, Bruce Ravel, and Joseph Woicik from NIST, and John Fabijanic, Zhong Zhong, and Howard Robinson from the Photon Sciences Department of BNL. It also consists of members of FMB Oxford, Scott Mowat, Andrew Fairley, Steve Siew, and Nigel Boulding.

Advisors to the beamline consist of the following:

Simon Bare, SSRL (Chair)

Andy Dent, DLS

Tien-Lin Lee, DLS

Mahalingam Balasubramanian, APS

Jose Rodriguez, BNL Chemistry

Dean DeLongchamp, NIST

Stuart Wilkins, NSLS-II, CSX

Tony Olhausen, Sandia

Joo Kang, DOW

Igor Levin, NIST

2 SST beamline

We describe the SST Beamline in terms of source, front-end, white- and pink beam sections, and the optics including mirrors, VLSPGM and DCM monochromators.

2.1 Source

The SST will be sited at 7-ID which is a low-beta straight section. The SST1 and SST2 will be served by two canted undulators with a 2 milli-radian canting angle. The SST1 undulator is an EPU60 out of vacuum undulator purchased from Wisconsin. The SST2 undulator is ESRF-U42 purchased from the ESRF. The specifications of the undulators are shown below.

Table 2.1: SST undulator specifications.

Beamline	SST1&2 7-ID	
Branch	SST1	SST2
Type	EPU	U42
Source	SRC	ESRF
Magnetic Length	0.84 m (14 periods)	1.6 m (38 periods)
Canted	Y	
Cant angle	2.0 mrad	
Period	60 mm	42 mm
Minimum gap	20.5mm (14mm)	12 (11.5) mm
Peak field	V: ~0.79 (~1.02) T H: ~0.45 (~0.73) T	0.79 (0.82) T
Keff	V: 4.1 (5.7) H: 2.5 (4.1) Circ: 3.0 (4.7)	3.15 (3.27)
Energy Range	LH: 150 (80) eV - ~3 keV LV: 340 (150) eV - ~3 keV C: 250 (115) eV - ~1 keV	345 (325) eV - ~10 keV
Power total	LH: 1.4 (2.7) kW LV: 0.51 (1.36) kW C: 0.74 (1.8) kW	2.9 (3.2) kW
Max.power per unit solid angle	LH: 4.8 (6.7) kW/mr ² LV: 2.8 (4.7) kW/mr ² C: 1.35 (2.0) kW/mr ²	13.3 (13.8) kW/mr ²
Straight	Low beta	
Device center	D/S +1.25 m	U/S -1.25 m
Fan angle *1 (mrad H)	LH: 1.60 / 2.16 (2.14 / 2.67) LV: 0.85 / 1.35 (0.87 / 1.41) C: 1.52 / 2.03 1.96 / 2.49)	1.29 / 1.87 (1.34 / 1.90)
Fan angle *1 (mrad V)	LH: 0.86 / 1.40 (0.87 / 1.43) LV: 1.06 / 1.66 (1.59 / 2.16) C: 1.51 / 2.02 (1.95 / 2.47)	0.85 / 1.38

Gap scanning and other requirements	Require energy scanning at fixed polarizations.	Required for NEXAFS experiments (specs as SRX).
-------------------------------------	---	---

Note *1. The fan angles of the radiation quoted here are as seen at 16 m from the source, and taking into account the effects of the source length and the canting. For the EPU60, the worst case fan size is taken (linear polarization mode gives the worst case horizontal fan, but helical mode requires the largest vertical fan aperture). The two values quoted are for the points where the power density falls to values that are 1% and 0.1% of the central value. These fringe power loads are taken into consideration when designing the XBMP and fixed mask for the SST beamline frontend.

Simulation of the spectral flux of the U42 undulator is shown by the solid line in Fig. 2.1. The simulation assumes that a minimum undulator gap of 11.5 mm can be achieved. This will be verified during field plotting in mid-2016. At 500 mA ring current, the spectral flux is approximately 10^{15} ph/s/0.1%bw from 3 to 7 keV through the SST front-end fixed mask which has an opening of 0.5 mrad (H) by 0.3 mrad (V).

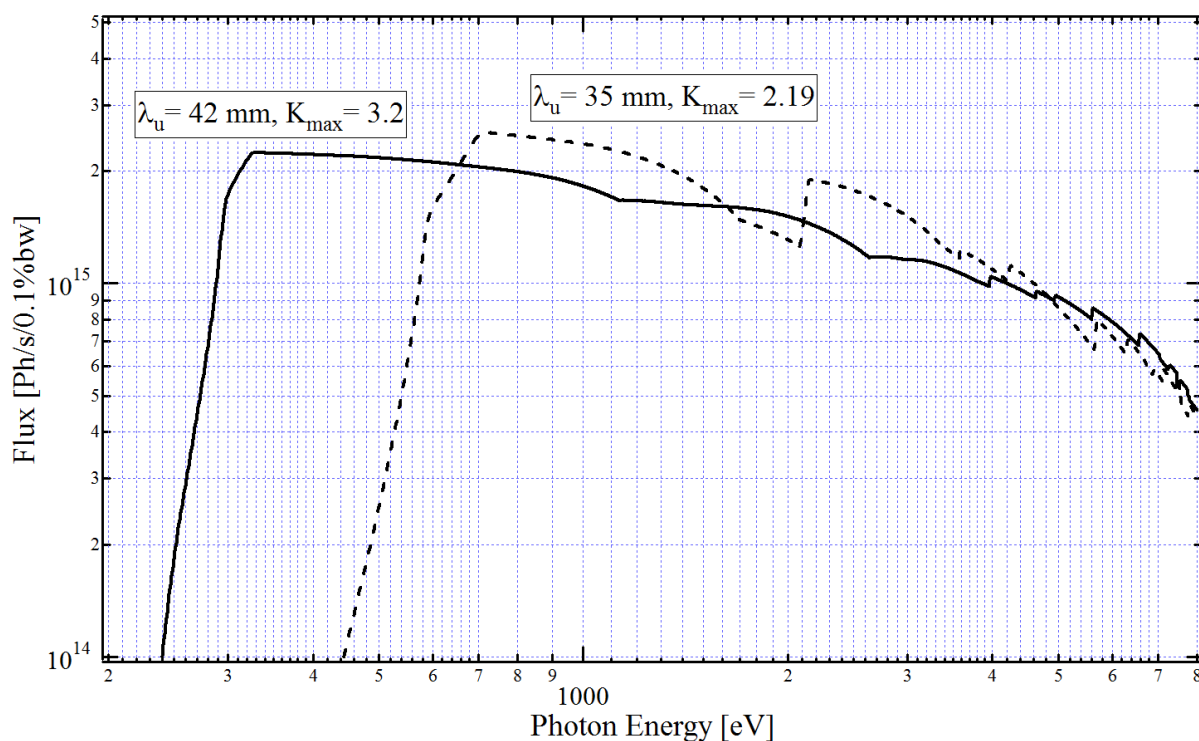


Figure 2.1: Spectral flux of U42 collected through 0.5 mrad (H) x 0.3 mrad (V) aperture. Min. undulator gap is assumed to be 11.5 mm. Peak field of 0.82 T is simulated using the measured remanent magnetization of $B_r=1.17$ T. A 1.6 m length is used for the simulation. Electron beam current is assumed to be 500 mA. The solid line represents the U42 device obtained from the ESRF. The dashed line represents expected flux from an alternative undulator of 35 mm period.

The spectral flux for linear horizontal and vertical polarization, and circular polarization of the EPU60 undulator is shown in Fig. 2.2. Note that the simulation assumes an aperture of 0.3×0.3 mrad which is less than the SST actual front-end mask of 0.5 (H) $\times 0.3$ (V) mrad. At 14 mm minimum expected gap, the undulator delivers approximately 10^{15} ph/s/ 0.1% bw through the fixed mask at about 100 eV. This gap value may require re-shimming of the magnets. At the conservative gap of 20.5 mm that the undulator was successfully operated under at the SRC, the linear horizontally polarized photons are at about 150 eV with a flux through the fixed mask of approximately 10^{15} ph/s/ 0.1% bw.

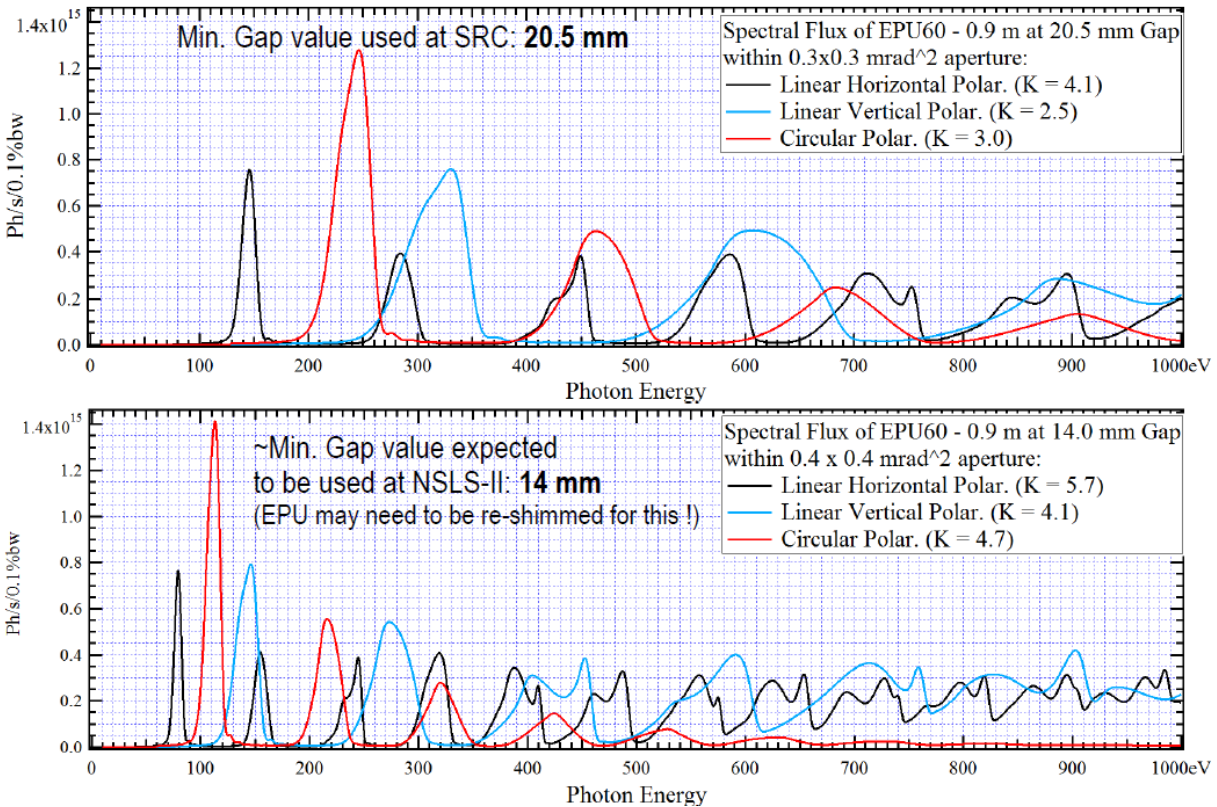


Figure 2.2: Spectral Flux of EPU60 through apertures comparable to to actual SST front-end aperture of 0.5 (H) \times 0.3 (v) mrad², assuming 20.5 and 14.0 mm gaps.

The EPU60, manufactured by ADC, was received in November 2014 at the NSLS-II. Photos of the undulator are shown in Fig.2.3. The control system is currently being upgraded to a Delta-Tau based motor driver to meet the NSLS-II standard before being tested by the NSLS-II insertion-device group for magnetic performance.



Figure 2.3: Photos of the EPU60.

The U42 undulator, pictured in Fig. 2.3, as received from the ESRF. It uses 5-phase motors. The control system upgrade will involve changing the motors to a newer 3-phase motor and gearbox, currently the standard at the ESRF for its U42 undulators, and purchasing of motor drivers for the 3-phase motors. As with most NSLS-II undulators, a Delta-Tau brick controller will provide pulse-direction signals to the 3-phase motor driver. A new absolute linear encoder system will be designed and procured to measure the gap. The U42 device will be tested by the NSLS-II insertion-device group for magnetic properties after the control systems upgrade.

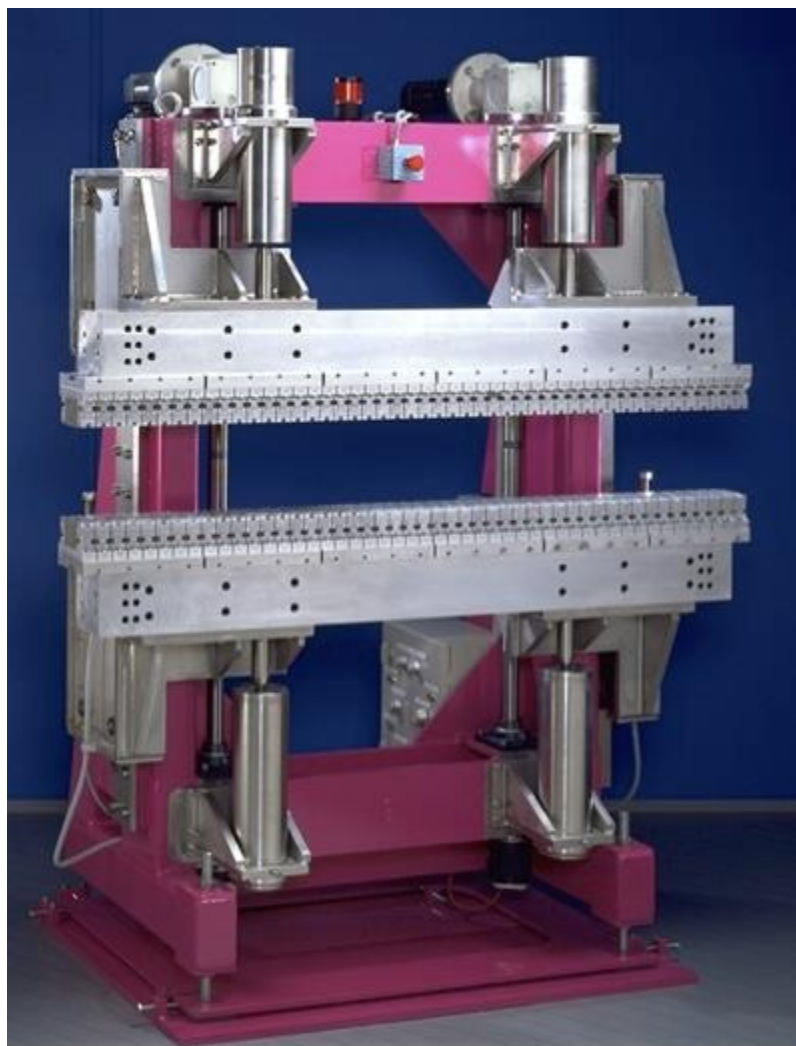


Figure 2.4: Picture of a standard ESRF U42 undulator.

Note that the SST beamline design assumes peak power densities of 6.7 kW/mrad^2 and 13.8 kW/mrad^2 for the EPU60 (SST1) and U42 (SST2), respectively. The maximum power through the $0.3 \times 0.5 \text{ mrad}^2$ front end fixed aperture is 1.01 kW for SST1 and 2.07 kW for SST2. The power density and total power for both devices are less than those of the NSLS-II IVU undulators and damping wiggler. Fig. 2.5 shows that the power density for the project-beamline insertion devices at NSLS-II is above 60 kW/mrad^2 , and masks are designed for 100 kW/mrad^2 . Thus, we can rely on experiences gained by the facility beamlines to guide our optical design, especially regarding heat-load management.

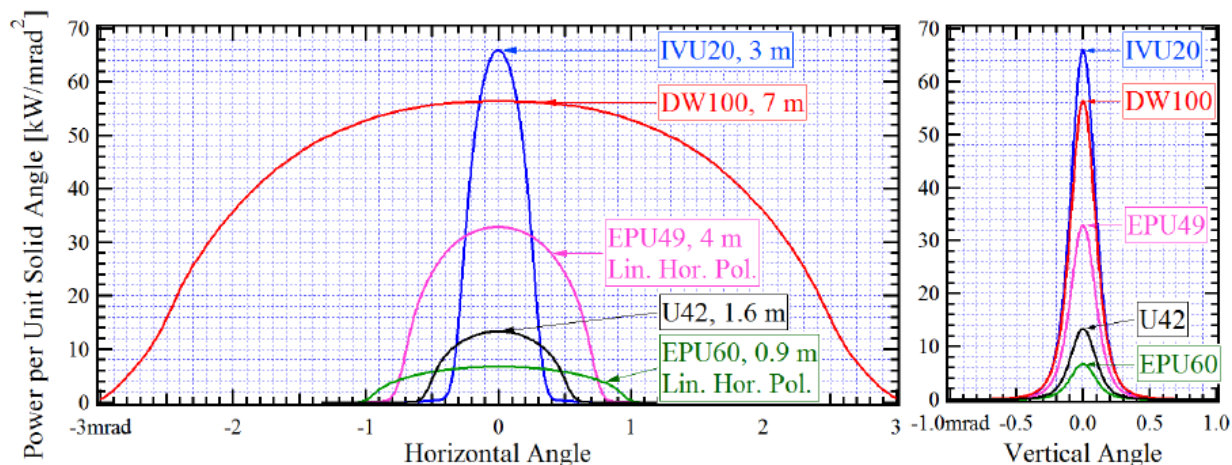


Figure 2.5: Power load variation with horizontal and vertical divergence of EPU60 and U42, along with that of DW100, IVU20 and EPU49 that are used by the NSLS-II project beamlines.

Figure 2.6 shows the straight-section layout of the SST beamline. The centers of the undulators are at 1.25 m from the center of the ID straight. The U42, located upstream of the ID center, is canted 1 mrad outboard. The EPU60, downstream of the ID center, is canted 1 mrad inboard.

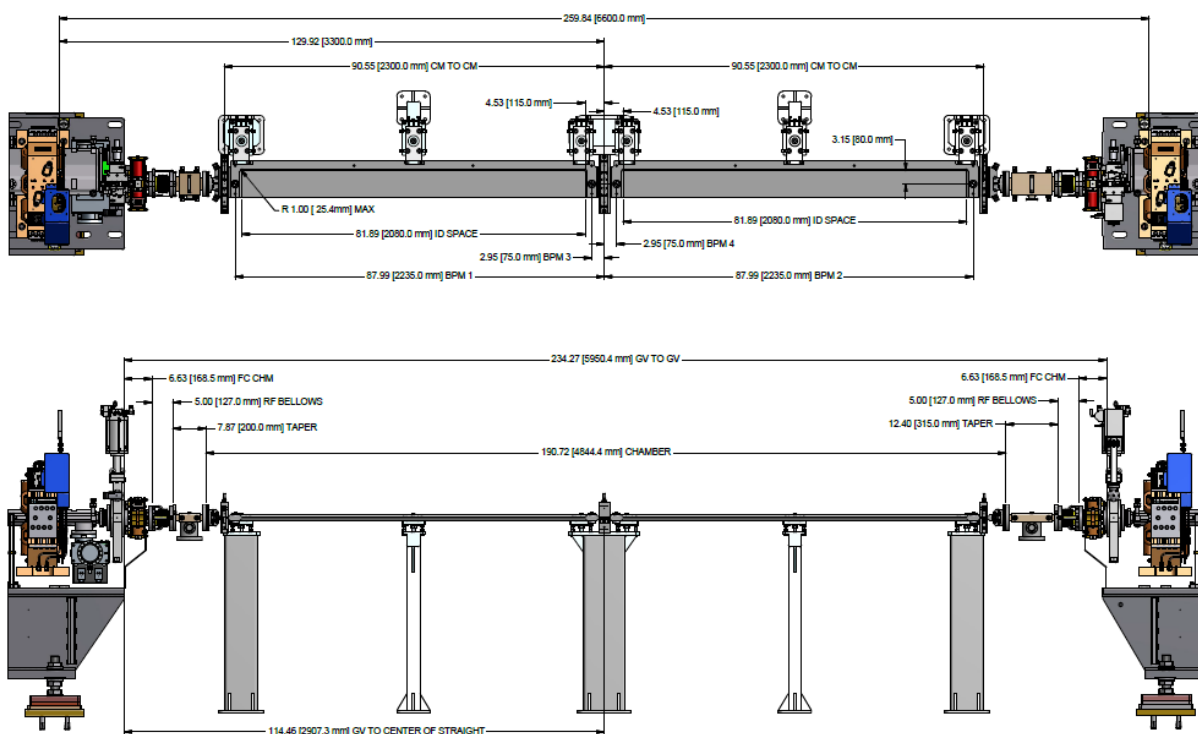


Figure 2.6: Design of the SST ID straight section.

2.2 Front End

The front end of SST is also similar to the standard NSLS-II front end design, with the opening angle customized to be 0.3 (V) x 0.5 (H) milli-radians for both undulators. Specifications for the front end components are shown in Table 2.2. Each undulator beam will be defined by its own X-Y slits. No mirrors are planned for the front-end.

Table 2.2: SST front-end component specifications.

		SST	
Photon shutter (BMPS)		Y	
Slow Gate Valve (SGV)		Y	
Beam Position Monitor 1 (XBPM1)		Y	
Beam Position Monitor 2 (XBPM2)		Y	
Fixed Aperture Mask (FAPM)		Y	
Type	Dual		
Source	EPU	IVU	
Vertical aperture (mrad)	0.3	0.3	
Horizontal aperture (mrad)	0.5	0.5	
Shape	Corner Radius	Corner Radius	
Bremsstrahlung Collimator BC1		Y	
Water Cooled Beryllium Window		N	
Fast Gate Valve (FGV)		Y	
Number of X-Y Slit sets (Two means both BLs of a canted pair have separate X-Y slits)		2	
Mirror System		N	
Fixed Mask 2		N	
Gate Valve		N	
Diagnostics Cross		N	
Photon Shutter (PS)		Y	
Bremsstrahlung Collimator BC2		Y	
Safety Shutter (x2)		Y	
Cycles per year required	5000		
Ratchet Wall Collimator		Y	
Ratchet Wall Modification		N	
Gate valve outside Ratchet Wall.		Y	

The layout of the SST front-end at 7-ID of the NSLS-II is shown in Figure 2.7.

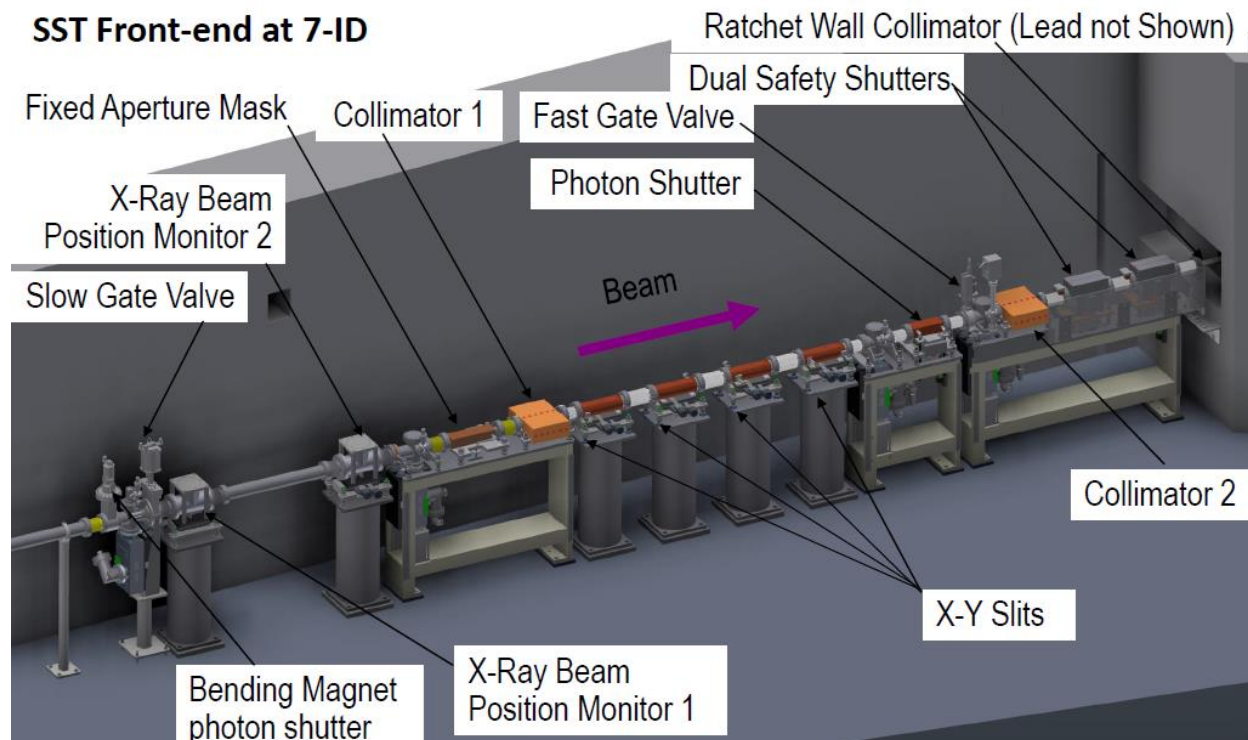


Figure 2.7: SST front-end configuration. Note that SST has two sets of X-Y slits to independently control the apertures of the two canted undulator beams. The two branches share the same front-end photon shutter and safety shutters.

SST will utilize a new fixed dual-aperture mask, shown in Fig. 2.8, to provide radiation fans to the FOE. The mask is at approximately 17 m from the source; each of its dual apertures is 0.5 mrad H and 0.3 mrad V. The aperture sizes for the EPU60 and U42 differ slightly due to the source location difference. The new design uses CuCrZr alloy which is considerably less expensive than Glidcop and more readily available, and uses only vertical tapering so that the region between the two apertures is passively safe for possible mis-steered undulator beams. The CuCrZr alloy allows for an integral conflat flange, thus eliminating the need for brazing a stainless-steel flange to the Glidcop mask, an undesirable feature in the old design. The mask will be tapered to safely absorb possible mis-steered undulator beam on the tapered surface. The vertically tapered beam-intercepting surface features internal fins to improve thermal efficiency.

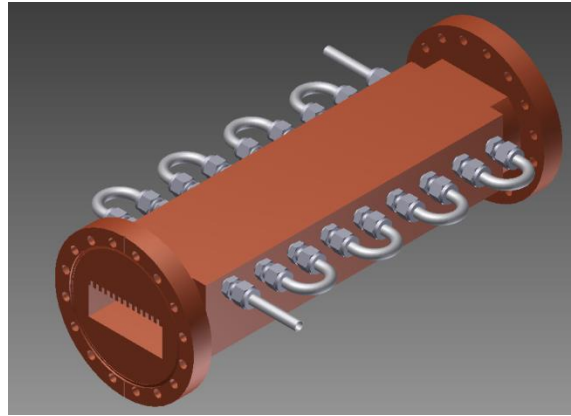


Figure 2.8: Design concept of the new front end fixed aperture mask. SST will be the first beamline at the NSLS-II to utilize this new design.

Simulations performed by Sushil Sharma show that this design keeps the water-cooled surface below 300°C at a normal-incidence power density of 103 kW/mrad². The resulting temperature and stress distribution are shown in Figure 2.9. It is assumed that the full beam is intercepted by the mask. This is a worst-case scenario which accounts for any mis-steering of the beam. Compared to the assumed 103 kW/mrad², the maximum power per unit solid angle at SST is much less at 13.8 kW/mrad² for SST2 (U42) and 6.7 kW/mrad² for SST1 (EPU60, horizontally polarized). Thus we are confident that the design of the fixed mask is conservative for SST.

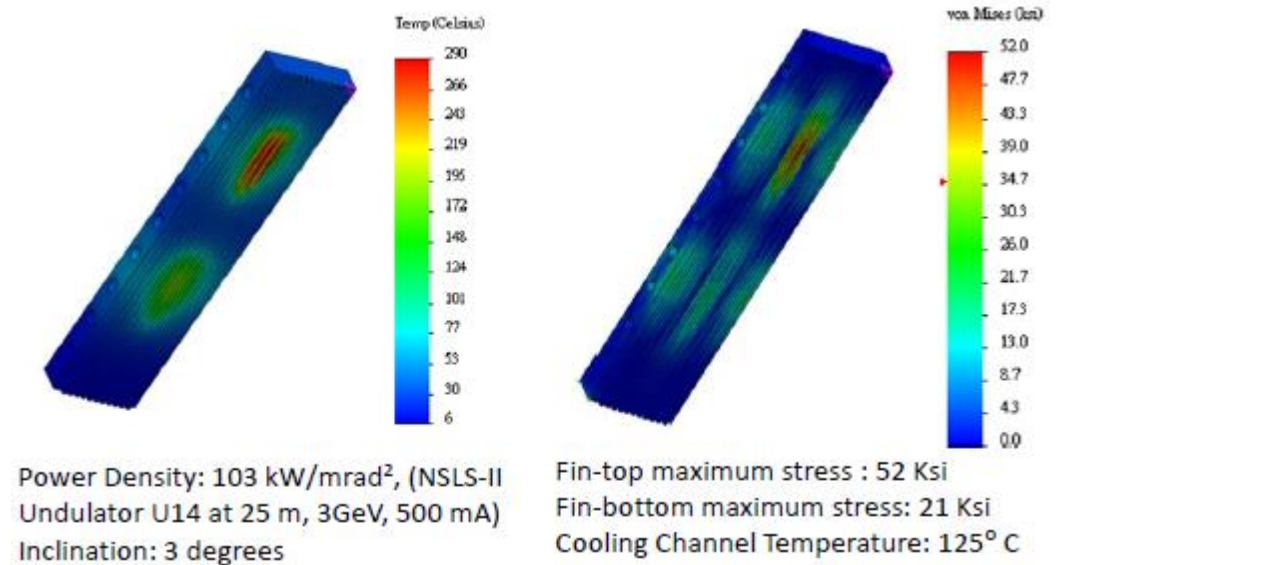


Figure 2.9: Parameters and FEA result for the SST front-end fixed aperture mask

pressure drop, will dump the electron beam in the storage ring, thus protecting the fixed mask from thermal damage. Once the ray-tracing drawings are finalized, a PPS aperture will be designed by Mary Carlucci-Dayton to protect the SST fixed cooled mask, discussed next.

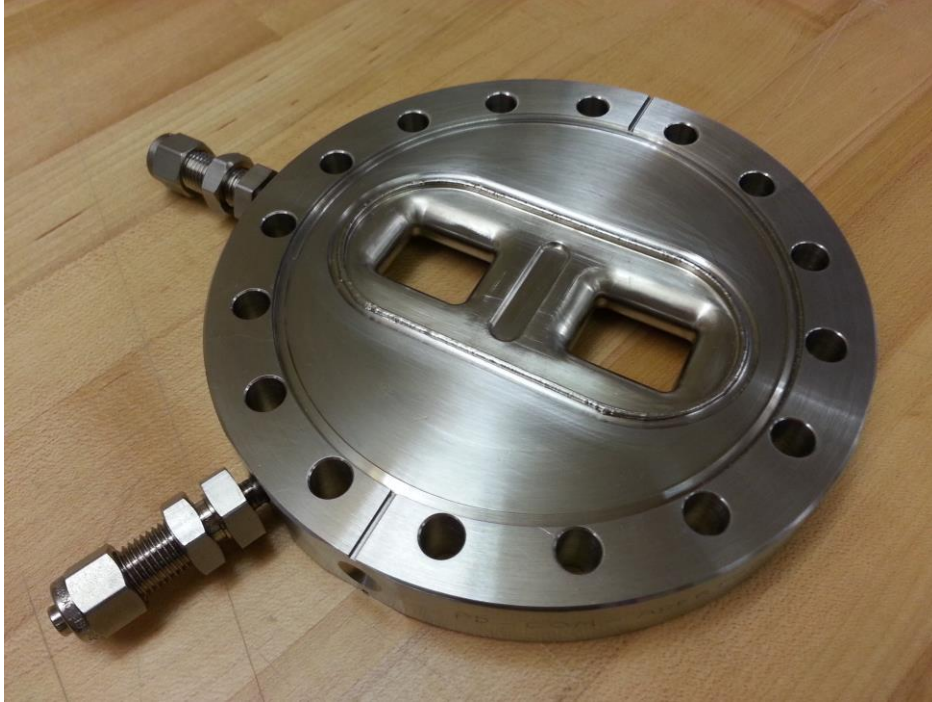


Fig 2.11: Picture of a typical dual-aperture PPS aperture.

Fixed cooled Mask

The water-cooled fixed mask aperture will be manufactured from Glidcop which will serve as the impingement surface. The heatload from the incident beam is distributed across a large surface area by the use of grazing incidence geometry. The compound angle principle is used to define the shape of the absorber such that the narrow part (i.e. the defining edge of the absorber) of the vertical defining edge of the grazing incidence surface does not coincide with that of the narrow part of the horizontal defining edge. This design minimizes the thermal stresses by eliminating the corner occurring when 2 intersecting surfaces meet. These corners are always subjected to high heat loads and are commonly the initiation point for stress corrosion cracking. A rendering of the fixed mask assembly is shown below in Fig.2.12.

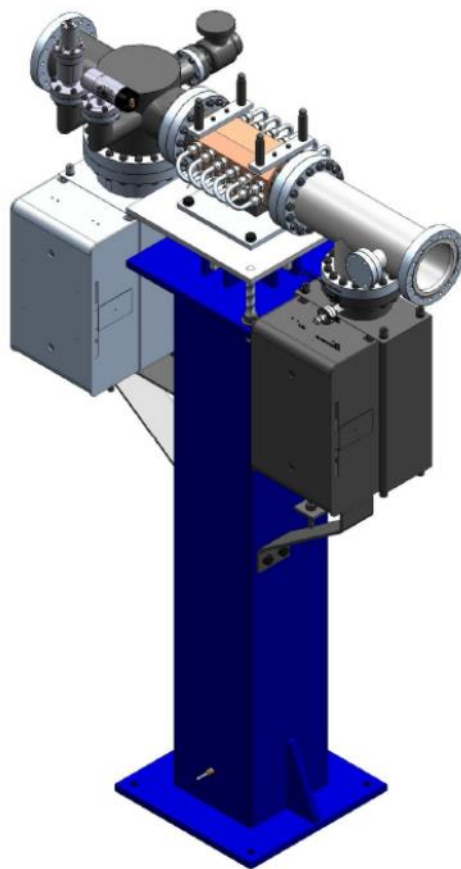


Fig 2.12: Fixed mask assembly designed by FMB-Oxford.

The Glidcop block is cooled by a series of water channels running across the block along the length of the unit. Water cooling channels pass through the Glidcop body, terminating in Swagelok fittings.

The cooled mask has an aperture for each beamline. Aperture sizes are 7.14mm x 7.14mm (0.27 mrad x 0.27 mrad) on the soft x-ray beamline and 7.14 mm x 4.76 mm (0.27 mrad x 0.18 mrad) on the tender branch. A 2 3/4" port is available for fitting of a fast valve sensor on the vessel above the 150 liter ion pump. Figure 2.13 shows the design of the fixed mask. The tapering angle of about 1 degree vertical, and 1.85 degrees horizontal is less than the 1.6 and 3.9 degrees used for the XPD front end fixed mask. Thus we are confident of the ability of the fixed mask to absorb the power. FEA of the temperature and stress distribution will be performed by FMB-Oxford for the worst case scenario in which the full U42 undulator beam is mis-steered onto the horizontal and vertical tapered surface.

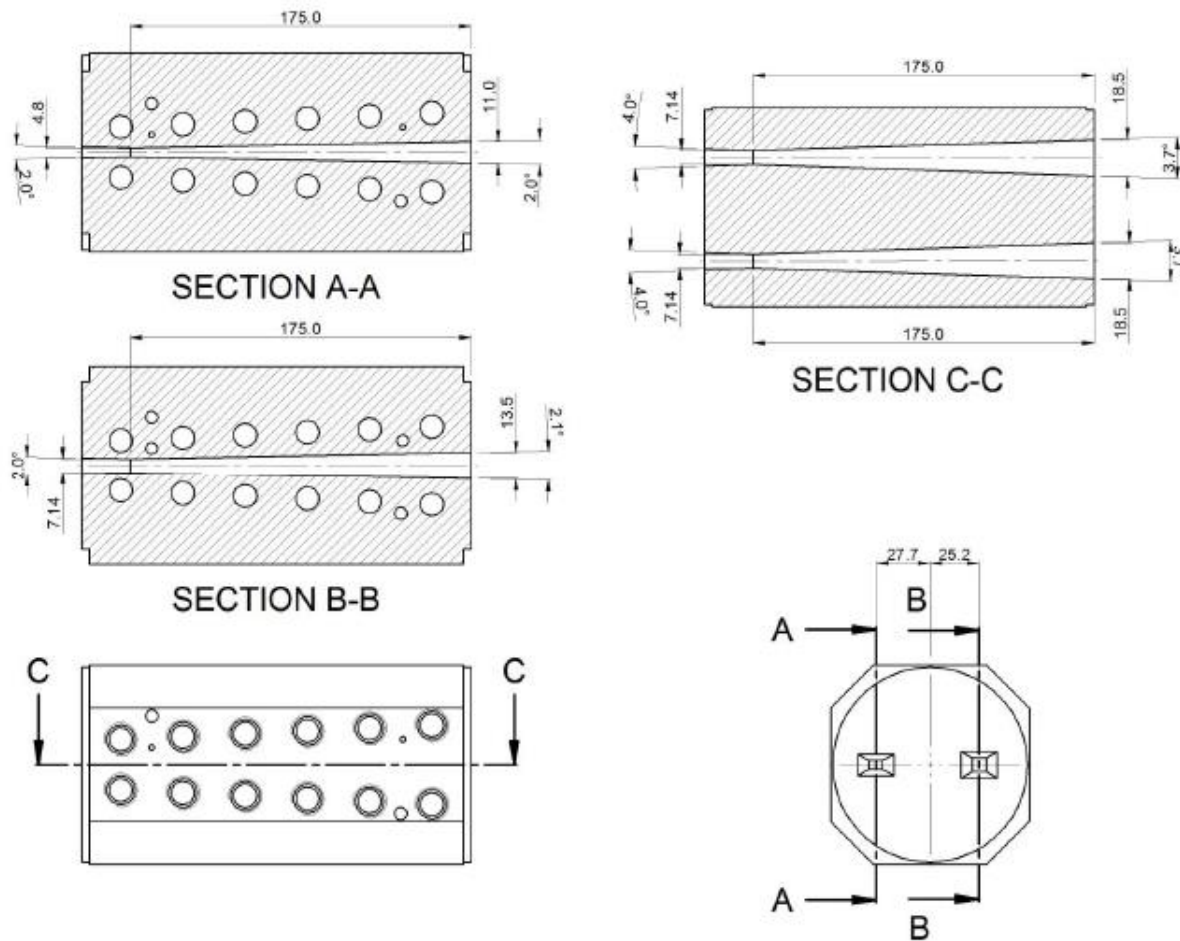


Fig 2.13. Design of the fixed mask.

White Beam Diagnostic Module

The white beam diagnostic module contains the BS Collimator, White Beam Stop, Vertical and Horizontal Slits. The BS Collimator, White Beam Stop, Vertical and Horizontal Slits of the White Beam Section are mounted on conflat flanges on the one vacuum vessel with manual adjustments provided. The manual adjusting stage is in turn secured to the synchrotron floor by a mild steel frame. Figure 2.14 illustrates the white beam diagnostic module.

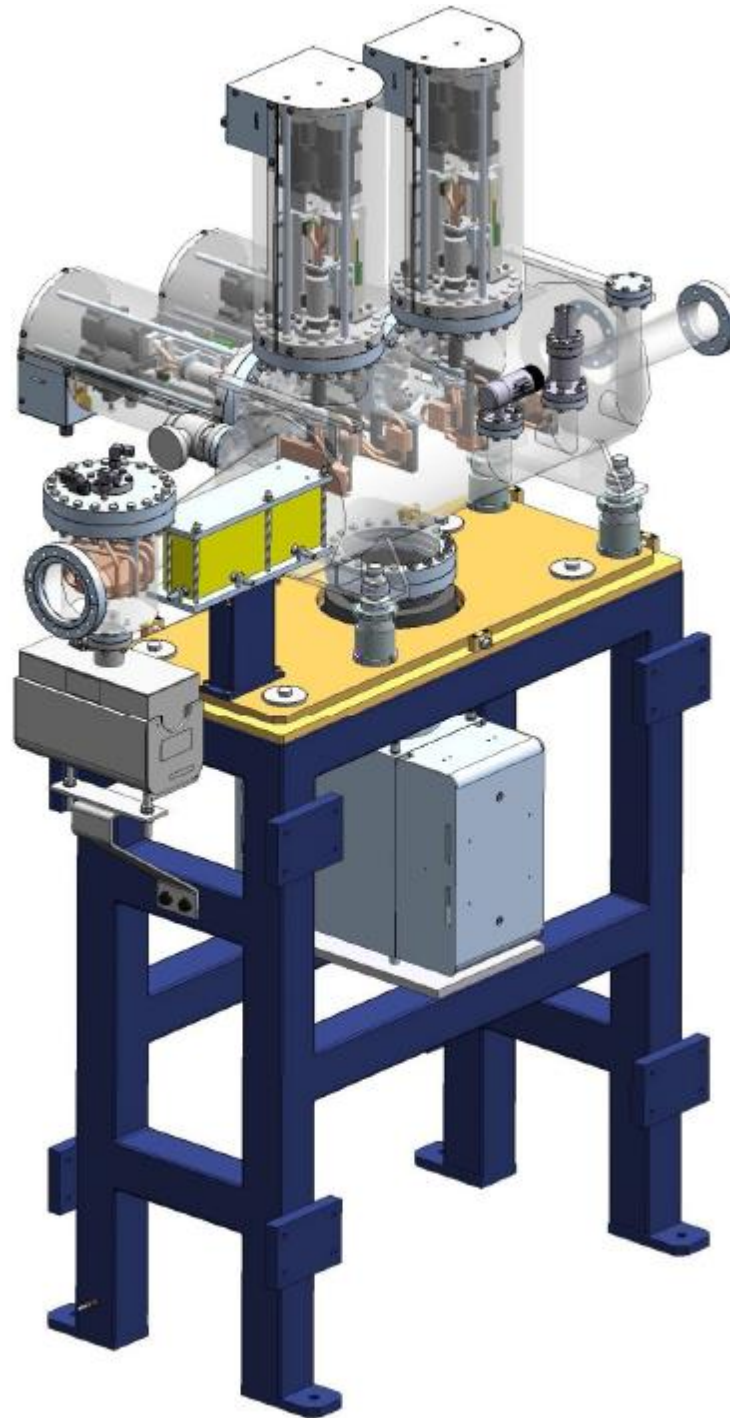


Fig 2.14: White beam diagnostic module. It resides after mirrors L1 and M1 as well as after the water-cooled mask.

Pink Beam Slits

There are two independent pink-beam slits servicing SST1 and SST2. Each pink-beam slit unit comprises two independently actuated slit blades, mounted on the same flange. Each slit system has a horizontal slit unit and a vertical slit unit, each of which is mounted on a flange on a vacuum vessel, one on top of the vessel and one at the side of the vessel. Each pair of blades defines either the horizontal or vertical dimension of the beam. The blades are manufactured from 4mm thick Tungsten. Fig.2.15a shows the design of the pink beam slits.

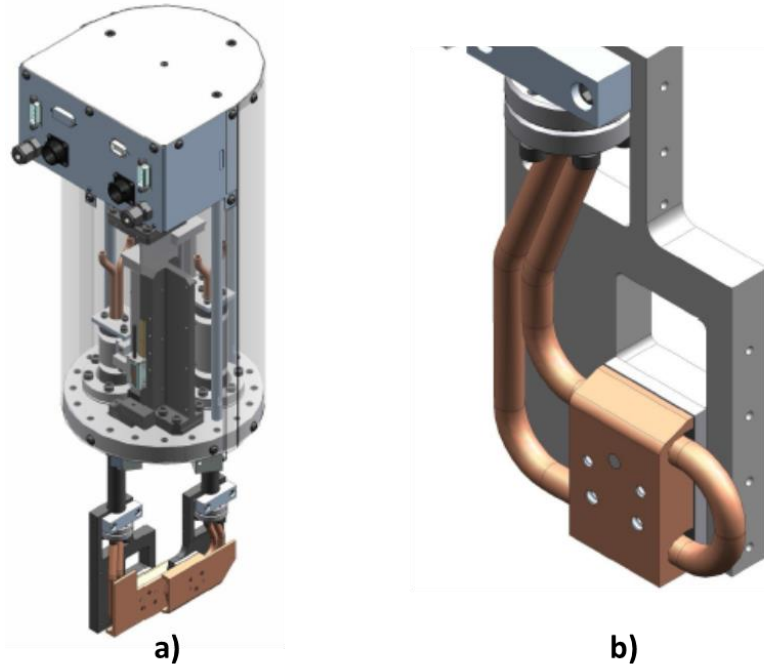


Fig 2.15: Design of the pink beam slits: a) assembly, b) details showing cooling block and slit blade arrangement.

Each cooled-slit unit consists of two slit blades, each of which is mounted onto a water-cooled body and connected to an external actuator mechanism through a flange on the slit vessel. The blade masks are constructed from Glidcop and have a 5° degree grazing incidence slope to reduce the power density of the beam on the block at the operating condition. The chamfered face is positioned on the upstream side of the block. A 25° steeper slope provides the heat absorbing surfaces that interact with the beam and withstand multiple applications of full power. The blade defining edge protrudes 0.5 mm above the cooling block. Fig.2.15b shows the cooling block and slit blade arrangement.

2.4 Beamline Optics

The optical layout is designed to accommodate a total of six experimental stations (see Table I). Two of the stations can be illuminated with soft and tender x-rays, three only with soft x-rays, and one only with tender x-rays. The two common stations could be illuminated with both IDs at the same time if an experiment requires two different photon energies over a wide energy range. Table 2.3 lists the expected size of the beam at the experimental stations.

Table 2.3: Experimental stations, their sources, and expected spot sizes The spot sizes are calculated assuming the soft ID is tuned to 200 eV with the medium energy grating and a 20 micron exit slit, and the tender ID is tuned to 1.5 keV.

Experimental stations	source	Spot size HxV (FWHM) mm ²	Un-focused Spot size HxV (FWHM) mm ²
HP NEXAFS	Tender	0.8x0.6 ^a	3.3x2.5 ^b
HAXPES/NEXAFS	Tender	0.1 x0.016 ^a	4.0 x 3.0 ^b
	Soft	0.064x0.031	0.45x0.43 ^c
Micro-XPS microscope	Tender	0.015x0.002	
	Soft	0.014x0.005	
HP NEXAFS/Fluorescence Yield	Soft	2.1x2.2	
NEXAFS/XPS	Soft	0.032x0.044	0.032x5 ^d
Micro-NEXAFS Imaging	Soft	1.1x1.2	20x20 ^e

a. L2A (toroid)

b. L2B (plain)

c. 0.1 degree yaw on M4A

d. Dithering M5C

e. Dithering M3C and M4D

Figure 2.16 shows the positions of the optical elements and experimental stations designed by the NIST team and further refined by the NIST team and FMB-Oxford. Rubin Reininger wrote the original detailed design report, shown in Appendix 1, for the optics.

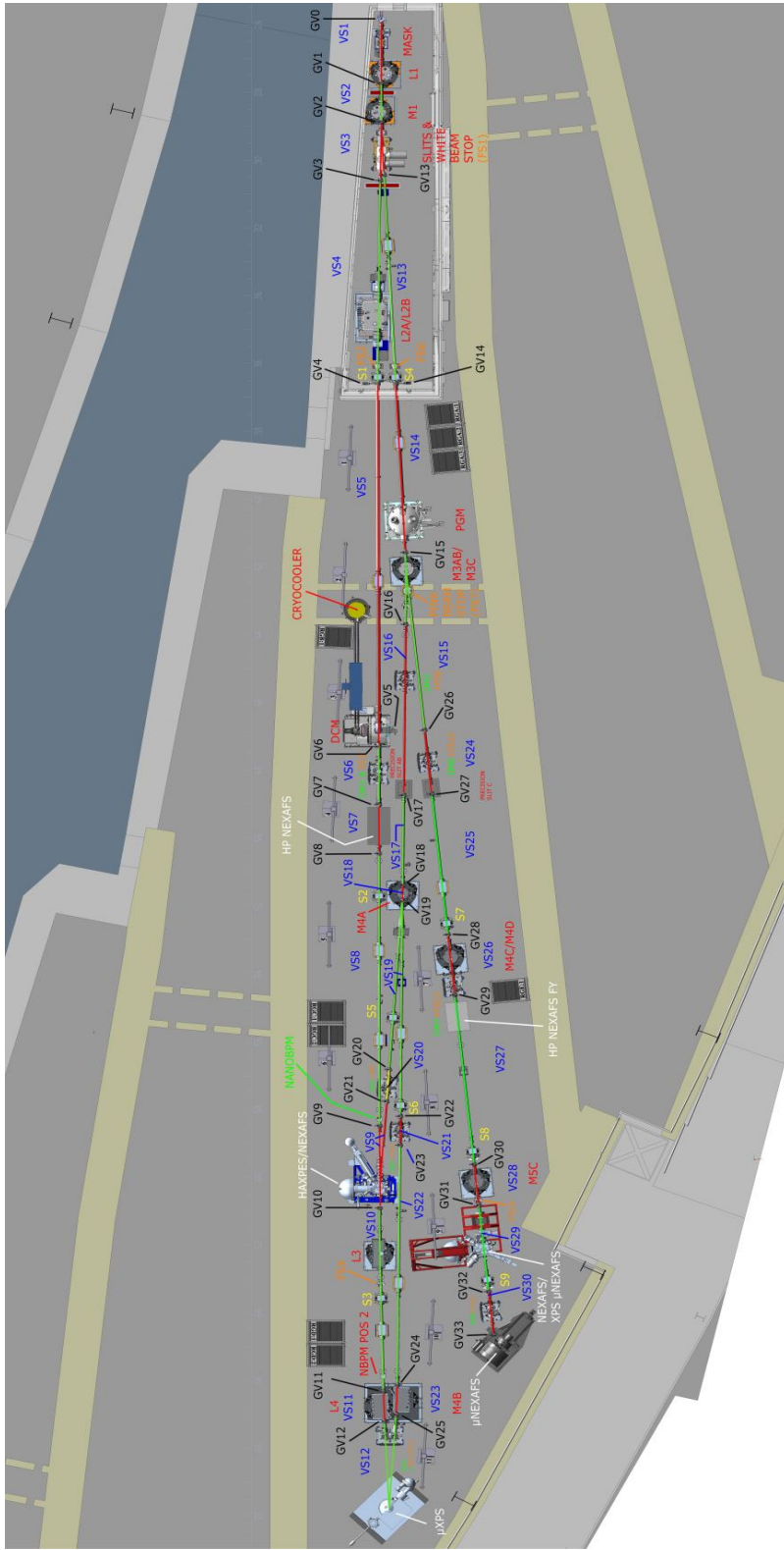


Fig 2.16: Optical design of SST beamline.

Characteristics of key optical components are discussed below. Each mirror system is mounted on an FMB Oxford hexapod. The motion specifications include pitch (R_y), Roll (R_z), and Yaw (R_x) ranges of ± 10 mrad. The pitch resolution and repeatability are < 1 micro-radians and < 5 micro-radians, respectively. The resolution and repeatability for both roll and yaw are < 5 and < 10 micro-radians, respectively. Vertical translation range is ± 20 mm with a resolution of < 1 micro-meter and repeatability of < 5 micro-meters. Lateral and longitudinal translation range is ± 5 mm with lateral resolution < 1 micro-meter and lateral repeatability < 5 micro-meters and longitudinal resolution < 2 micro-meters and longitudinal repeatability < 10 micro-meters. Fig 2.17 shows the typical design of the mirror system, with the exception of M4 and L3B which is a double hexapod and shown in Fig. 2.18.

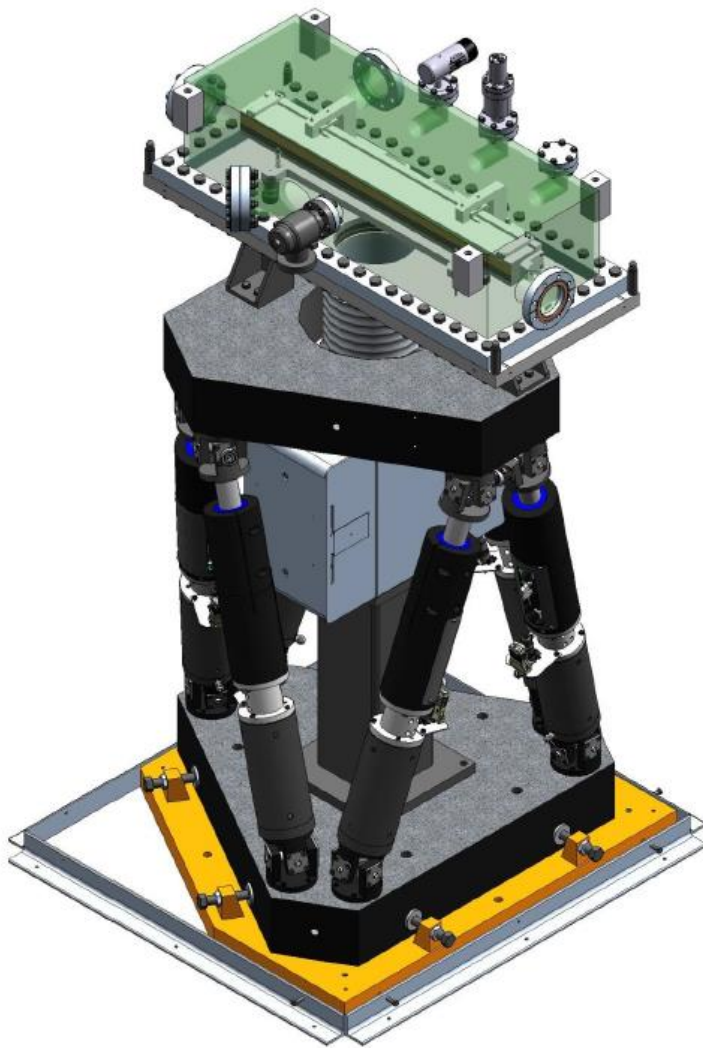


Figure 2.17: Typical FMB single hexapod mirror design.

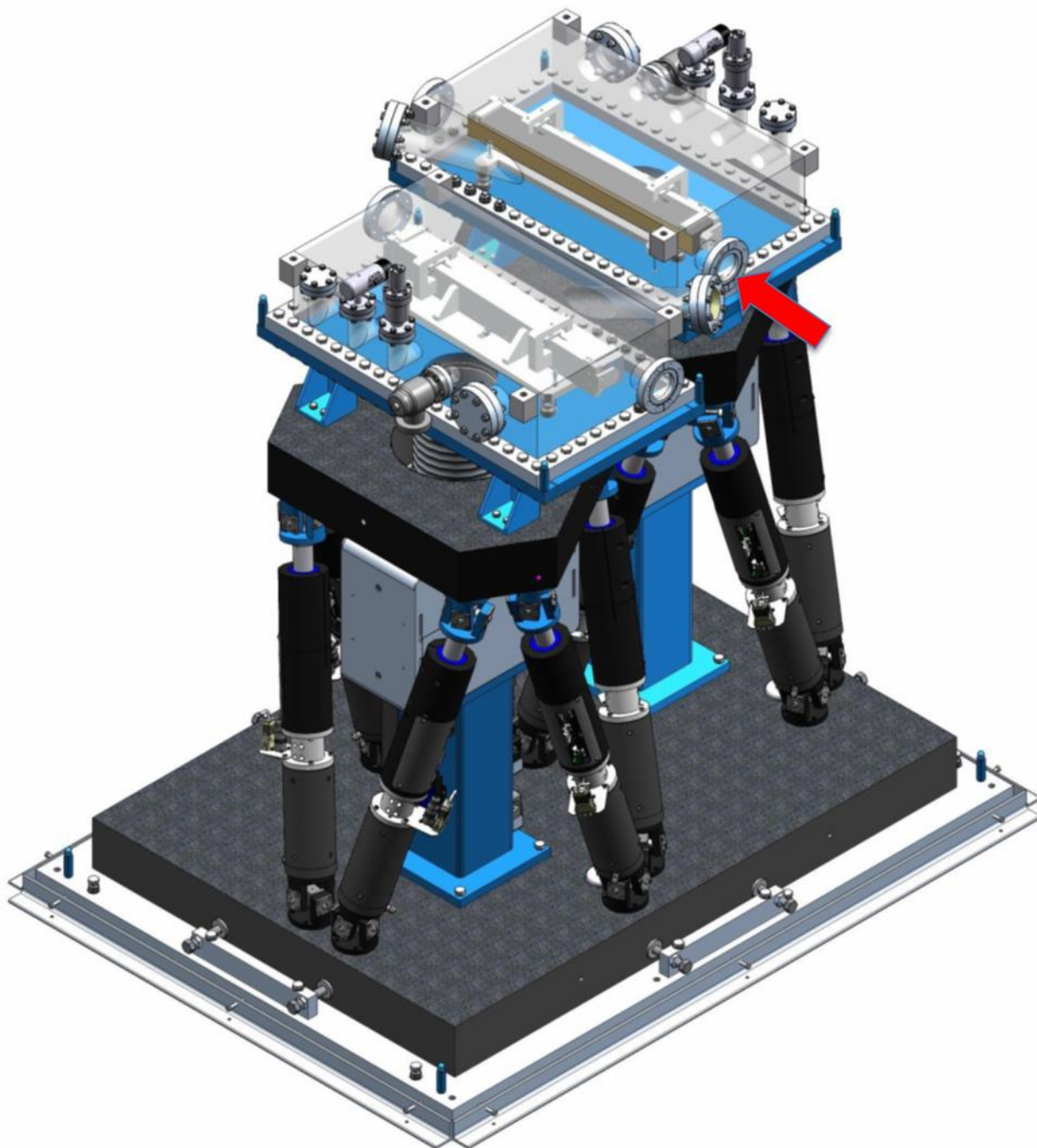


Figure 2.18: L4/M4B mirror system on a FMB double hexapod.

A. L1

The first optical element of the tender branch is a plane mirror deflecting the beam in the horizontal plane by 1.2 degrees. This mirror is water cooled and will absorb the power

emitted by the undulator at photon energies above the energy range covered by the tender x-ray branch. Beam footprint on the mirror is 305 mm x 2.4 mm. This mirror is inside the FOE.

Table 2.4: Specification of L1 mirror optic.

Substrate material	Single crystal silicon
Substrate dimensions	335 mm L x 60 mm W x 60 mm D
Active area	285 mm x 43 mm
Grazing incidence angle	0.6 degrees
Substrate shape	Planar, tangential radius > 30 km, sagittal radius > 3 km
Tangential slope error	<0.2 micro-radians RMS
Sagittal slope error	<2 micro-radians
Coating	Au 300 Å ± 10% thick 20 mm wide Ni 300 Å ± 10 % thick 20 mm wide Under layer chrome binder thickness 100 Å ± 25 Å
Surface roughness	<3 Å RMS
Surface quality	0.5 scratches or points per cm ² over 99 % of active optical area
Cooling	Internally water cooled

B. L2A and L2B

L2A and L2B are a pair of interchangeable mirrors that deflect the tender beam in the horizontal plane by 1.2 degrees. L2A is a toroidal mirror which focuses the radiation onto the sample position of the HAXPES/NEXAFS station with a demagnification of approximately 1.2:1. L2B is a plain mirror deflecting the radiation towards the μ XPS station. Both mirrors are side cooled. Either of these mirrors can be used for the high

pressure (HP) NEXAFS station. Beam footprints on the mirrors are 350x2.7 mm². The mirrors are located inside the FOE.

Table 2.5: Specification of L2A mirror optic.

Substrate material	Single crystal silicon
Substrate dimensions	400 mm L x 60 mm W x 60 mm D
Active area	350 mm x 43 mm
Grazing incidence angle	0.6 degrees horizontally deflecting outboard, horizontally and vertically focussing
Substrate shape	Toroidal Tangential radius 2.41 km \pm 1.5 % Sagittal Radius 265 mm \pm 1 %
Tangential slope error	<1 micro-radians RMS
Sagittal slope error	<5 micro-radians RMS
Coating	Au 300 Å \pm 10% thick 20 mm wide Ni 300 Å \pm 10 % thick 20 mm wide
Surface roughness	<3 Å RMS
Surface quality	0.5 scratches or points per cm ² over 99 % of active optical area
Cooling	Side water cooled

Table 2.6: Specification of L2B mirror optic.

Substrate material	Single crystal silicon
Substrate dimensions	400 mm L x 60 mm W x 60 mm D
Active area	350 mm x 43 mm
Grazing incidence angle	0.6 degrees horizontally deflecting outboard

Substrate shape	Planar Tangential Radius > 30 km Sagittal Radius > 3 km
Tangential slope error	<0.2 micro-radians RMS
Sagittal slope error	<2 micro-radians RMS
Coating	Au 300 Å ± 10% thick 20 mm wide Ni 300 Å ± 10 % thick 20 mm wide
Surface roughness	<3 Å RMS
Surface quality	0.5 scratches or points per cm ² over 99 % of active optical area
Cooling	Side water cooled

C. Tender X-ray Monochromator

The crystals in the double crystal monochromator (DCM) diffract vertically. The DCM will be illuminated by a converging beam when L2A is used, and by a diverging beam when L2B is used. The beam divergence for photon energies higher than 1.5 keV with either mirror is less than 0.1 mrad. The monochromator offset is 15 mm. The first crystal of the monochromator requires liquid nitrogen cooling. The monochromator uses interchangeable Si(111), Si(220), and YB66 crystals.

D. L3

L3 is a plane mirror used to guide the tender beam to the sample position of the μ XPS station. L3 deflects the photon beam in the horizontal plane by 1.2 degrees. The mirror deflects horizontally outboard. Since L3 and L4 are placed after the monochromator, they do not require water cooling. Beam footprint on L3 is 660 x 5.5 mm². The optical location for L3 relative to the center of the straight section is x=-40.33 mm, y=15 mm, and z=62258 mm.

The specification for L3 mirror is shown in Table 2.7

Table 2.7: Specification of L3 mirror optic.

Substrate material	Single crystal silicon
Substrate dimensions	670 mm L x 50 mm W x 60 mm D
Active area	660 mm x 30 mm
Grazing incidence angle	0.61 degrees
Substrate shape	Planar, tangential radius > 20 km, sagittal radius > 3 km
Tangential slope error	<0.25 micro-radians RMS
Sagittal slope error	<5 micro-radians RMS
Coating	Au 300 Å±10% thick, 21 mm wide over 100 Åchrome binder layer C 300 Å ±10% thick, 21 mm wide over chrome binder layer
Surface roughness	<3 Å RMS
Surface quality	0.5 scratches or points per cm ² over 99 % of active optical area
Cooling	uncooled

E. L4

L4 is an ellipsoidal mirror that focuses the tender x rays onto the sample position of the μ XPS station. It images the source with a demagnification of approximately 23:1. Beam footprint on the mirror is 720 x 5.7 mm². L4 optics is uncooled. The L4 mirror is mounted to the base of its vacuum vessel and is manipulated using a hexapod which gives six degrees of freedom. Since L4 and M4B mirrors are both located upstream of the μ XPS station, in close proximity to each other, they vacuum chambers share the same base plate. Figure 2.15 shows the design of L4 and M4B mirror system.

Table 2.8: Specification of L4 mirror optic.

Substrate material	Fused Silica
Substrate dimensions	600 mm L x 50 mm W x 60 mm D
Active area	540 mm x 6 mm
Grazing incidence angle	0.61 degrees
Substrate shape	Ellipsoidal Major axis 35509.4 mm \pm 1% Minor axis 152.8 mm \pm 1% Mirror pole X_m (off axis) 32509.7 mm \pm 1%
Tangential slope error	<2.0 micro-radians RMS
Sagittal slope error	<10 micro-radians RMS
Coating	Au 300 Å \pm 10% thick, 15 mm wide
Surface roughness	<3 Å RMS
Surface quality	0.5 scratches or points per cm ² over 99 % of active optical area
Cooling	uncooled

F. M1

M1 is the first optical element of the soft branch. It is a plane mirror deflecting the EPU beam in the horizontal plane by 3.0 degrees. This mirror will be water cooled and will absorb the power emitted by the EPU at photon energies above the range covered by the

soft x-ray branch. M1 is inside the FOE and is the only optical element for the soft branch that is located in the FOE. Beam footprint on the mirror is 183 x 4.3 mm².

Table 2.9: Specification of M1 mirror optic.

Substrate material	Single crystal silicon
Substrate dimensions	250 mm L x 70 mm W x 60 mm D
Active area	200 mm x 60 mm
Grazing incidence angle	1.5 degrees
Substrate shape	Planar, tangential radius > 30 km, sagittal radius > 3 km
Tangential slope error	<0.2 micro-radians RMS
Sagittal slope error	<2 micro-radians
Coating	C 300 Å ± 10 % thick 19 mm wide Au 300 Å ± 10 % thick 16 mm wide Ni 300 Å ± 10 % thick 19 mm wide Under layer chrome binder thickness 100 Å ± 25 Å on full area
Surface roughness	<3 Å RMS
Surface quality	0.5 scratches or points per cm ² over 99 % of active optical area
Cooling	Internally water cooled

G. Soft x ray VLS PGM monochromator

The principles of the VLS PGM monochromator are described by R. Reininger et. al. Rev. Sci. Ins. **79**, 033108 (2008). The major difference here is that the beam incident on M2 along the vertical direction is diverging and not vertically collimated as in the CSX beamline described in the paper above. The plane mirror (M2) in front of the gratings will be internally water-cooled and the gratings will be side cooled to avoid performance impairment due to the absorbed power density. The chosen gratings have line densities of 250 (LEG), 600 (MEG) and 1200 (HEG) lines/mm at their centers and are operated with c

values (defined as $\cos\beta/\cos\alpha$, where α is the angle of normal incidence and β is the diffraction angle) of 1.5, 1.5 and 2.0, respectively. The expected resolution with an exit-slit width of 20 microns and taking into account state of art slope errors on the optical elements is given in Fig. 2.19. Reducing the exit slit to 10 microns improves the energy resolution by a factor of between 1.3 and 1.8 in all gratings.

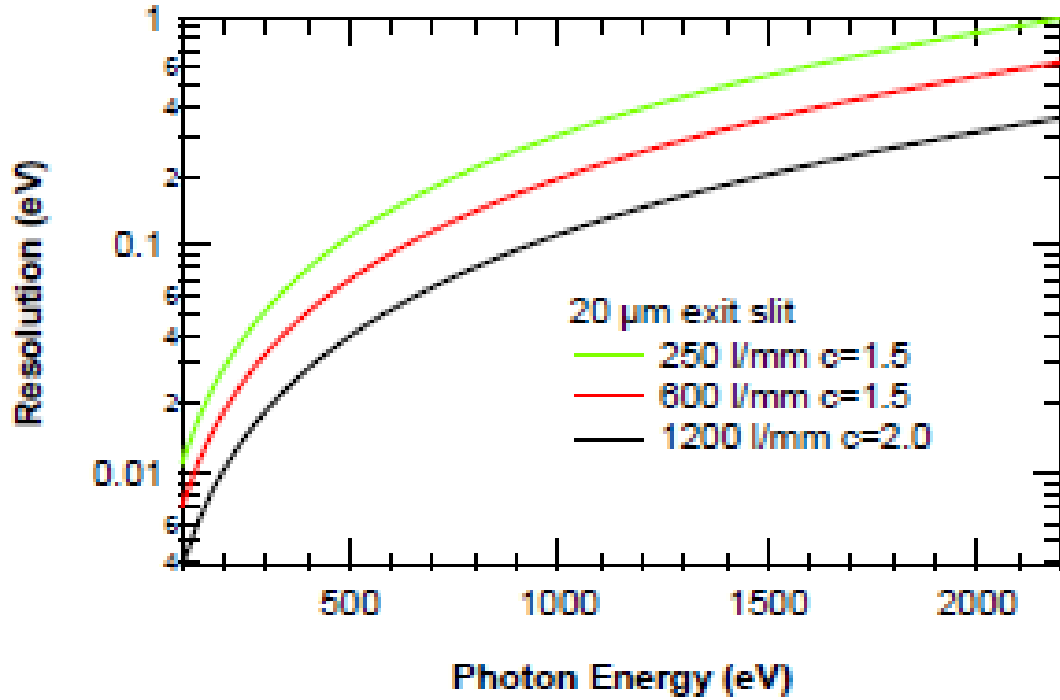


Figure 2.19: Expected resolution with the three gratings assuming an exit slit with width of 20 microns.

The variation of line densities and groove parameters are listed in Table 2.10.

Table 2.10: Grating parameters. The groove density variation is given by $k(\omega) = k_0(1 + 2b_2\omega + 3b_3\omega^2 + \dots)$, where ω is positive towards the exit slit.

Grating	c mm ⁻¹	k ₀ mm ⁻¹	b ₂ 10 ⁻⁴ mm ⁻¹	b ₃ 10 ⁻⁸ mm ⁻²	Coating	Blaze or trapezoidal angle (degrees)	Groove depth (nm)	Groove width (microns)

LEG	1.5	250	2.451	2.75	Au	28	20	2.4
MEG	1.5	600	2.450	2.75	Au	28	8	1.0
HEG	2	1200	1.749	2.06	Au	0.9		

H. M3AB and M3C

Both M3AB and M3C are elliptical cylinders focusing the beam along the horizontal direction at the corresponding exit slit. The demagnification of both mirrors is the same 4.3:1. Only one mirror will intercept the beam at any given time. M3AB deflects the beam horizontally inboard by 3.5 degrees, towards the tender endstations (HAXPES-NEXAFS and μ XPS). M3C deflects the beam horizontally outboard by 3 degrees towards the soft branch. The beam footprints on M3AB and M3C are 234x8 mm² and 273x8 mm², respectively. M3C is used to make a 20 mm wide spot at the μ NEXAFS station by dithering it \pm 0.22 mrad.

Table 2.11: Specification of M3AB mirror optic.

Substrate material	Fused Silica
Substrate dimensions	280 mm L x 60 mm W x 40 mm D
Active area	230 mm x 45 mm
Grazing incidence angle	1.75 degrees deflecting beam inboard towards M4A and M4B
Substrate shape	Tangential Ellipse Major axis 23665.1 mm \pm 1% Minor axis 497.5 mm \pm 1% Mirror pole 17168.6 mm (off axis) Z \pm 1% Sagittal Radius > 3km
Tangential slope error	<1.0 micro-radians RMS
Sagittal slope error	<10 micro-radians RMS
Coating	C 300 Å \pm 10 % thick 13 mm wide

	Au 300 Å ± 10% thick 13 mm wide Ni 300 Å ± 10 % thick 13 mm wide
Surface roughness	<3 Å RMS
Surface quality	0.5 scratches or points per cm ² over 99 % of active optical area
Cooling	uncooled

Table 2.12: Specification of M3C mirror optic.

Substrate material	Fused Silica
Substrate dimensions	310 mm L x 60 mm W x 40 mm D
Active area	270 mm x 45 mm
Grazing incidence angle	1.5 degrees deflecting beam outboard to M4C and M4D
Substrate shape	Tangential Ellipse Major axis 23664.9 mm ± 1% Minor axis 426.4 mm ± 1% Mirror pole Xm (off axis) 17167.8 mm ± 1% Sagittal Radius > 3km
Tangential slope error	<1.0 micro-radians RMS
Sagittal slope error	<10 micro-radians RMS
Coating	C 300 Å ± 10 % thick 13 mm wide Au 300 Å ± 10% thick 13 mm wide Ni 300 Å ± 10 % thick 13 mm wide
Surface roughness	<3 Å RMS
Surface quality	0.5 scratches or points per cm ² over 99 % of active optical area
Cooling	uncooled

I. M4A

M4A is an ellipsoidal mirror deflecting the beam horizontally by 3.5 degrees inboard towards the HAXPES/NEXAFS station on the tender branch. It magnifies the beam at the exit slit by 1:2.9 onto the sample position of the HAXPES-/NEXAFS station. The beam footprint on M4A is 108x3.5 mm². M4A can be retracted from the beam path to allow the incident beam to proceed to M4B.

Table 2.13: Specification of M4A mirror optic.

Substrate material	Fused Silica
Substrate dimensions	150 mm L x 25 mm W x 40 mm D
Active area	110 mm x 10 mm
Grazing incidence angle	1.75 degrees
Substrate shape	Ellipsoidal Major axis 5903.8 mm \pm 1% Minor axis 158.1 mm \pm 1% Mirror pole X _m (off axis) 2837.9 mm \pm 1%
Tangential slope error	<1.0 micro-radians RMS
Sagittal slope error	<10 micro-radians RMS
Coating	Au 300 Å \pm 10% thick 10 mm wide
Surface roughness	<3 Å RMS
Surface quality	0.5 scratches or points per cm ² over 99 % of active optical area
Cooling	uncooled

J. M4B

M4B is an ellipsoidal mirror that images the exit slit onto the μ XPS sample position with a demagnification of 5.6:1. M4B deflects the beam horizontally by 3.5 degrees inboard. The beam footprint on M4B is 650x21 mm².

Table 2.14: Specification of M4B mirror optic.

Substrate material	Fused Silica
Substrate dimensions	600 mm L x 60 mm W x 60 mm D
Active area	540 mm x 21 mm
Grazing incidence angle	1.75 degrees
Substrate shape	Ellipsoidal Major axis 10604.9 mm \pm 1% Minor axis 231.9 mm \pm 1% Mirror pole Xm (off axis) 7405.7 mm \pm 1%
Tangential slope error	<2.5 micro-radians RMS
Sagittal slope error	<10 micro-radians RMS
Coating	Au 300 Å \pm 10% thick 30 mm wide
Surface roughness	<3 Å RMS
Surface quality	0.5 scratches or points per cm ² over 99 % of active optical area
Cooling	uncooled

K. M4C

M4C is an ellipsoidal mirror that images the exit slit onto the sample position of the NEXAFS/XPS station with a 1:17 magnification. The mirror deflects the beam by 3.0 degrees in the vertical plane. The beam footprint on M4C is 225x5.5 mm². This mirror is interchangeable with M4D that is housed in the same vacuum vessel.

Table 2.15: Specification of M4C mirror optic.

Substrate material	Fused Silica
Substrate dimensions	270 mm L x 35 mm W x 50 mm D
Active area	230 mm x 15 mm
Grazing incidence angle	1.5 degrees
Substrate shape	Ellipsoidal Major axis 6835.9 mm \pm 1% Minor axis 172.4 mm \pm 1% Mirror pole Xm (off axis) -1836.6 mm \pm 1% Sagittal Radius > 3km
Tangential slope error	<2.0 micro-radians RMS
Sagittal slope error	<10 micro-radians RMS
Coating	Au 300 Å \pm 10% thick 15 mm wide
Surface roughness	<3 Å RMS
Surface quality	0.5 scratches or points per cm ² over 99 % of active optical area
Cooling	uncooled

L. M4D

M4D is a plane mirror that generates a large vertical spot at the μ NEXAFS station. Beam footprint on the mirror when M3C is being dithered horizontally to obtain a 20 mm spot at the μ NEXAFS station is 225x20 mm². This mirror is capable of dithering ± 0.43 mrad vertically to obtain a 20 mm tall spot at the μ NEXAFS station.

Table 2.16: Specification of M4D mirror optic.

Substrate material	Titania Silicate Low Expansion Glass
Substrate dimensions	250 mm L x 35 mm W x 50 mm D
Active area	230 mm x 20 mm
Grazing incidence angle	1.5 degrees
Substrate shape	Plane Tangential radius > 20 km Sagittal radius > 3 km
Tangential slope error	<0.25 micro-radians RMS
Sagittal slope error	<5 micro-radians RMS
Coating	Au 300 Å \pm 10% thick 15 mm wide over 100 Å chrome binder layer
Surface roughness	<3 Å RMS
Surface quality	0.5 scratches or points per cm ² over 99 % of active optical area
Cooling	uncooled

M. M5C

M5C is a plane mirror that deflects the beam to the NEXAFS/XPS station sample position. Its position and angle were determined by the need to re-use the present experimental

station. Taking the mirror out of the beam-path allows the beam into the μ NEXAFS station. Beam footprint on the mirror is $78 \times 1.3 \text{ mm}^2$. M5C is dithered by $\pm 0.62 \text{ mrad}$ to obtain a 5 mm vertical stripe at the sample of the NEXAFS/XPS station.

Table 2.17: Specification of M5C mirror optic.

Substrate material	Single crystal silicon
Substrate dimensions	120 mm L x 35 mm W x 30 mm D
Active area	100 mm x 15 mm
Grazing incidence angle	1.0 degrees
Substrate shape	Plane Tangential radius > 20 km Sagittal radius > 3 km
Tangential slope error	<0.25 micro-radians RMS
Sagittal slope error	<5 micro-radians RMS
Coating	Au $300 \text{ \AA} \pm 10\%$ thick 15 mm wide on 100 \AA chrome binder layer
Surface roughness	<3 \AA RMS
Surface quality	0.5 scratches or points per cm^2 over 99 % of active optical area
Cooling	uncooled

2.5 Radiation Shielding

First Optical Enclosure

The First Optical Enclosure (FOE) is designed to be white beam compatible and to shield against the Gas Bremsstrahlung (GB) radiation generated in the 7-ID beamline straight section. The NSLS-II guideline specifications for the first optical enclosure, "NSLS-II Guidelines for Beamline Shielding," were followed for the FOE design and lead thickness specification. Since the bremsstrahlung shielding requirement is more demanding than the synchrotron shielding requirement, there is no need for extra lead shielding due to the undulator source.

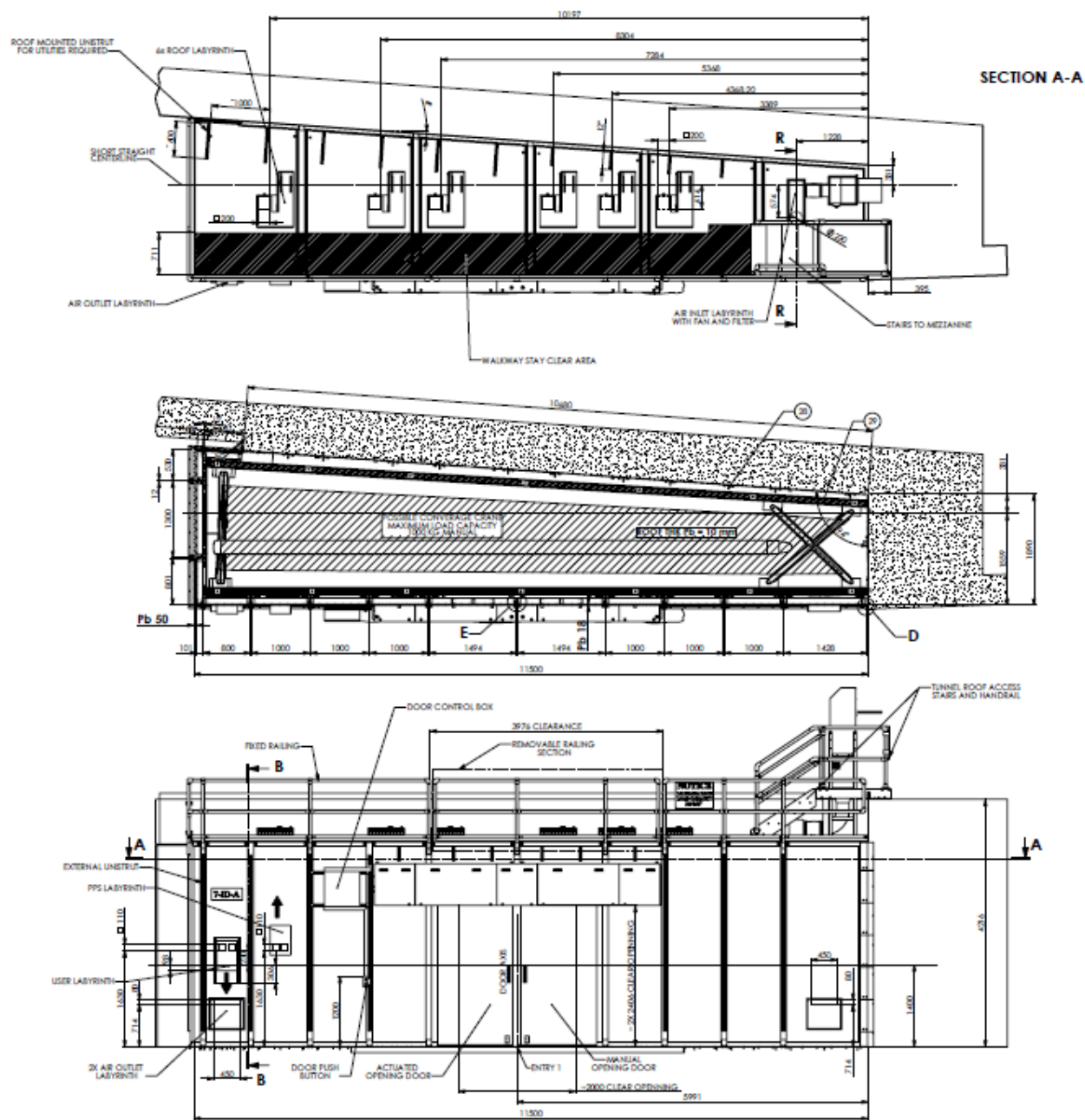


Fig 2.20: Design of the FOE.

The SST FOE, shown in figure 2.20, is designed with 18 mm-thick lead for the lateral and upstream panels, 50 mm-thick lead for the downstream panel, and 10 mm-thick lead for the roof. The endstations and transport pipes are shielded for monochromatic x rays following NSLS-II guidelines for radiation shielding.

Access to the roof of the FOE is via the roof of the storage-ring tunnel. Rails are designed to allow personnel access to the roof. Equipment racks for vacuum instrumentation and FOE-related motion control are placed on the experimental floor, in the three instrumentation racks located downstream of the FOE.

Ray tracing

Fig.2.21 shows preliminary ray tracing for Bremsstrahlung radiation in the horizontal plane. In addition to the frontend Bremsstrahlung collimators, one Bremsstrahlung collimator and two Bremsstrahlung stops (one of lead and one of tungsten) are needed in the FOE.

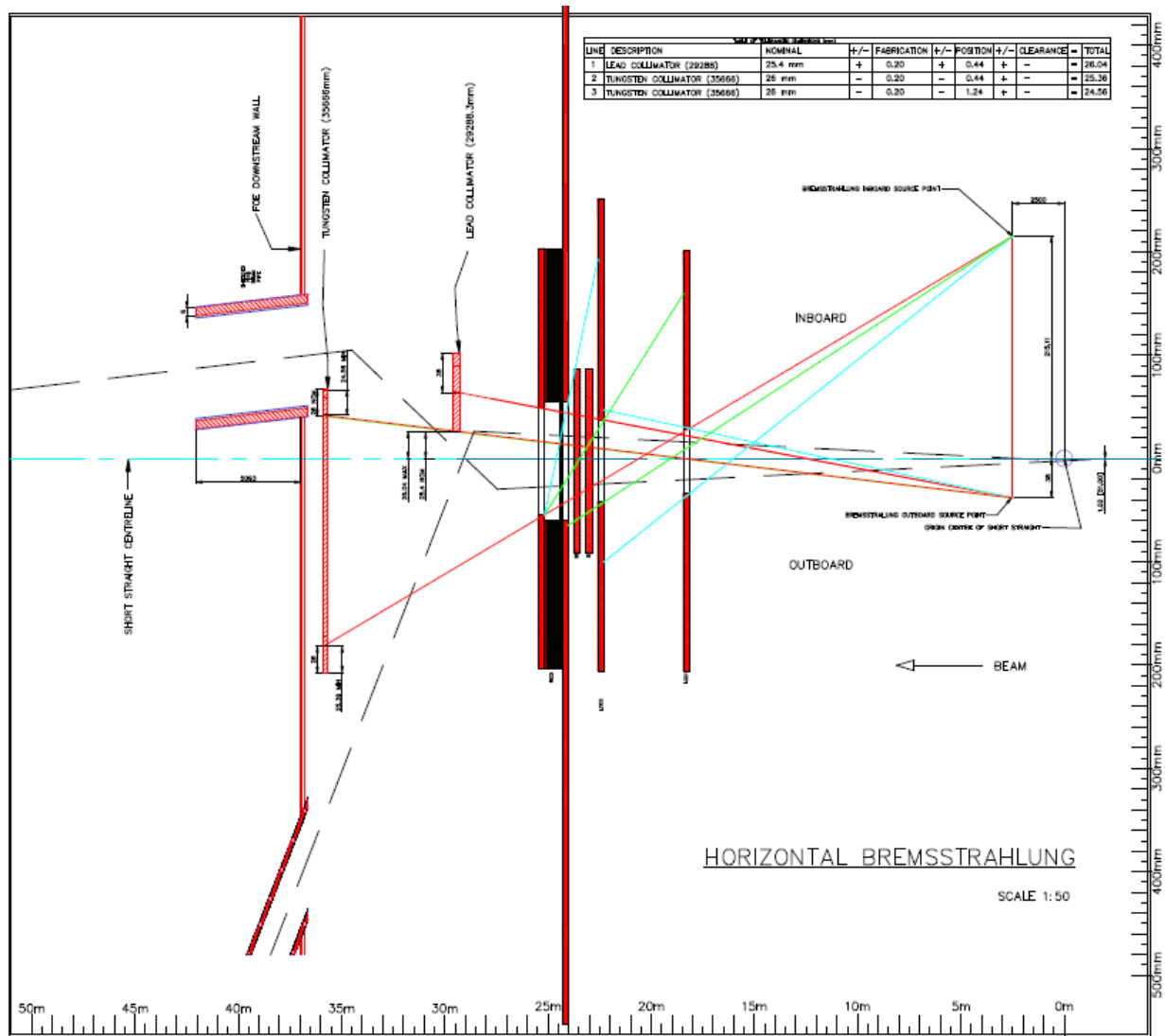


Fig 2.21: Preliminary Bremsstrahlung ray-tracing in the horizontal plane.

Fig.2.22 shows preliminary synchrotron ray-tracing for normal synchrotron beam in the horizontal plane.

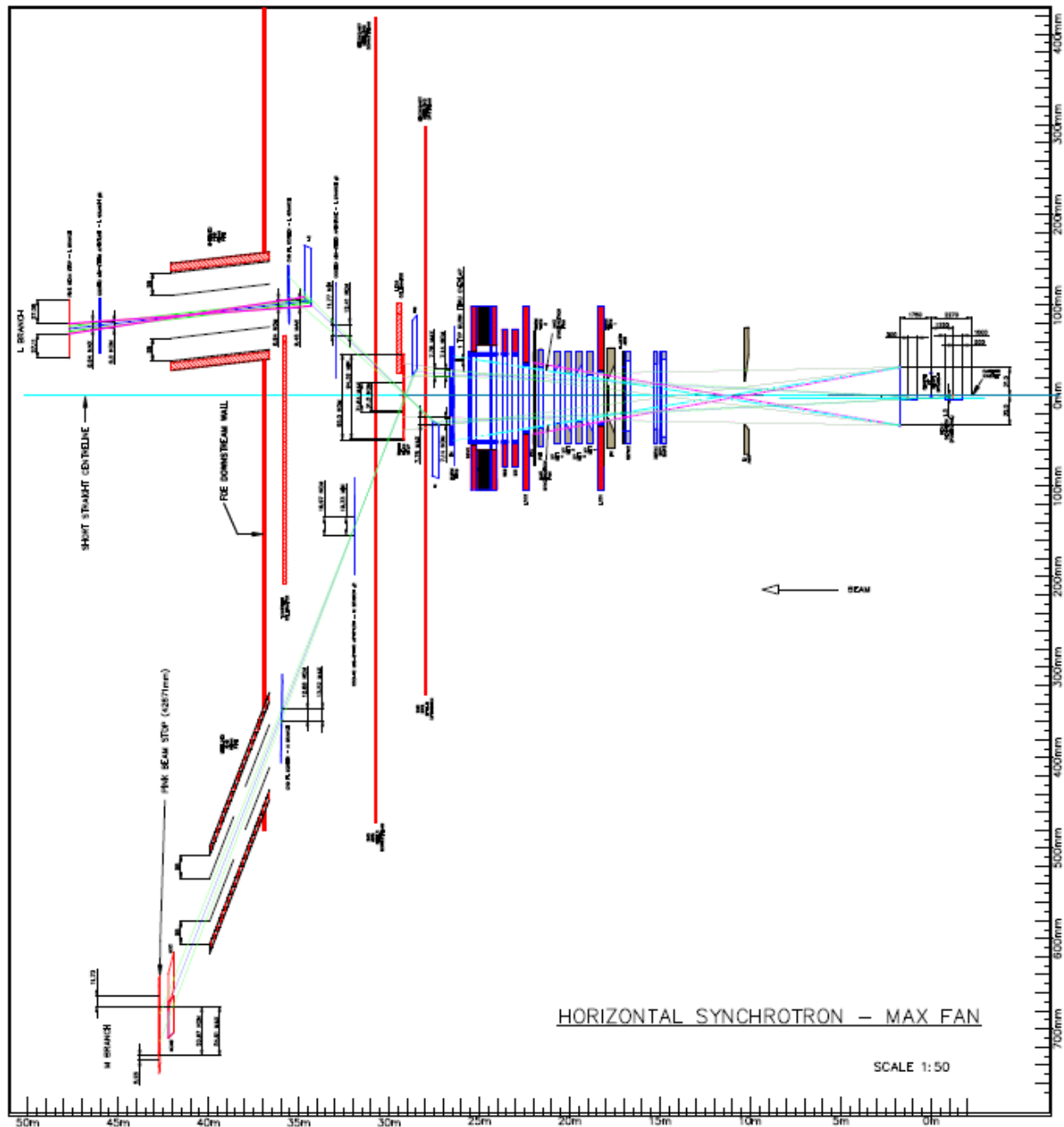


Fig 2.22: Preliminary synchrotron ray-tracing in the horizontal plane, showing the shielded beampipe.

Secondary Bremsstrahlung radiation shielding

The secondary Bremsstrahlung shields are designed according to the NSLS-II shielding guidelines. The main scatterers to be considered for Secondary Gas Bremsstrahlung (SGB) shielding analysis are: white beam mask, two white beam mirrors, and two white beam stops. To eliminate the need for exclusion zones such as that used by the CSX beamline, downstream of the FOE, a shielded beampipe is placed between the FOE and the tender x-ray double-crystal monochromator (DCM). A preliminary SGB design will be proposed using ray-tracing of 2, 4, and 8 degree angles from the straight centerline. We will then ask Mohamed Benerrouche to verify the effectiveness of the proposed secondary Bremsstrahlung shields and shielded beampipe via Monte-Carlo simulation using FLUKA code. The simulation results will be used to guide the final design for secondary Bremsstrahlung shields.

Lead and Tungsten Bremsstrahlung Stops

The purpose of the Bremsstrahlung stop is to ensure that the Bremsstrahlung radiation cannot exit the FOE, so that no primary Bremsstrahlung radiation shielding or exclusion zone is needed on the experimental floor. Two Bremsstrahlung Stops are required in the FOE.

The lead Bremsstrahlung stop will be manufactured from lead of density no less than 11340 kg/m^3 . The BS stop, shown in Fig.2.23a, is mounted outside of the vacuum on the diagnostic module stand and precisely aligned with respect to the beam. The stop is set using the manual adjustments available on the support. The size of the block is dictated by the Bremsstrahlung ray tracing.

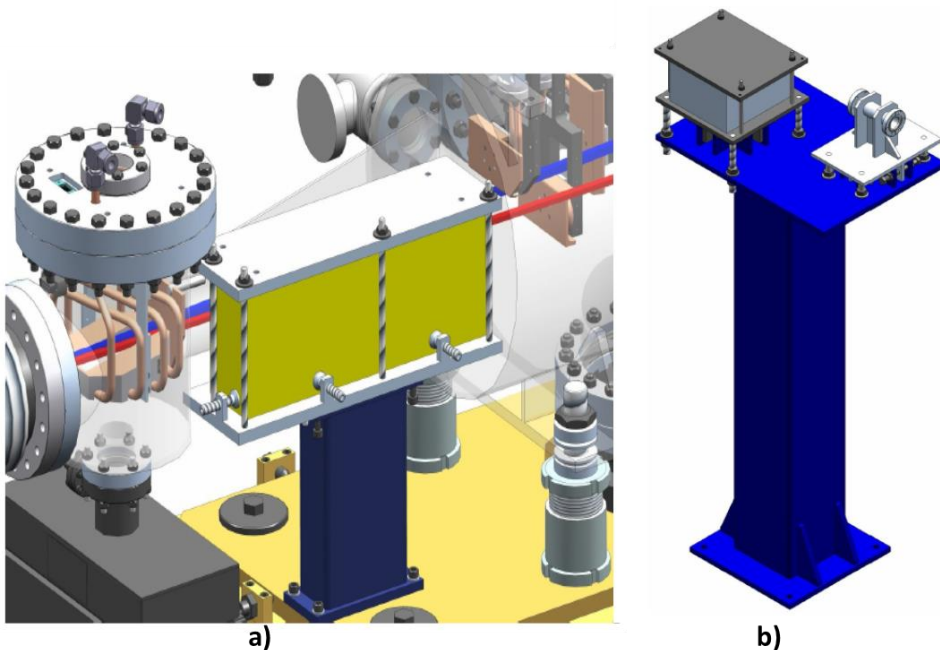


Fig 2.23: Designs of a) Lead b) Tungsten Bremsstrahlung stop.

The tungsten Bremsstrahlung stop is manufactured from non-magnetic tungsten alloy of density 17.8g/cm³. It is mounted outside of the vacuum on a stand and precisely aligned with respect to the beam. The stop is set using the manual adjustments available on the support. Fig.2.23b shows the design of the Tungsten BS stop.

Pink-Beam Transport Pipe

The PGM for SST1 and DCM for SST2 are both located on the experimental floor, receiving pink beam. The NSLS-II shielding policy did not specify the requirements for pink-beam transport, but recommends using white beam transport pipe specifications. Thus the transport pipes from the FOE to the monochromators will be shielded with 7 mm thick lead according to the requirements for white beam or according to the shielding calculations. The pink-beam transport pipe is sized along with an additional cooled pink-beam mask upstream of the DCM, so that no synchrotron rays, even under mirror mis-steering, can hit the transport pipe, and that pink beam is greater than 25 mm from the inside wall of the transport pipe according to the NSLS-II shielding policy for white beam.

Shielding for Monochromatic beam transport pipes and endstations

P. Berkvens performed simulations for shielding requirements at the SST. Assuming a 2m EPU58 for the soft branch, and a 2m IVU26 for the tender branch, he concluded that available steel-wall thickness is sufficient downstream of both the DCM and PGM monochromators. It is recommended that attention should be paid to viewing ports and over-pressure rupture disks on end stations and that a small on-axis beam stop may be necessary to terminate the beamline. Since the assumed undulators in the Berkvens study provide higher flux than the EPU60 (0.9m) and U42 (1.6m) used for SST and he assumed a 3.5 GeV ring energy, we are confident about the validity of the conclusions and recommendations, especially for the soft branch. Nevertheless, we have requested Mohamed Benerrouche to perform an independent study of the shielding requirements for beam transport pipes, monochromators, and the endstations of both branches with the complete final beamline configuration.

The monochromatic sections of the tender branch, having x rays of up to 7 keV, has been studied by Amy Xia. Three scenarios were considered in the simulation study: 1. Beam scraping a stainless

steel beampipe, to assure that the beam transport pipes are safe. 2. Beam scattering off a target in a stainless-steel chamber, to assure that the mirror chambers, diagnostic modules, and end-stations are safe. 3. Beam being stopped by a stainless steel beam-stop, to define the required beam-stop thickness. The assumptions and conclusions of the case studies are summarized below.

Scenario 1: Beam scraping 2 mm thick Fe pipe at 100 mrad angle: Dose rate is negligible outside of 2 mm SS pipe. The dose rate from STAC8 calculation is 5.83E-07 mrem/h after 2 mm Fe shielding. The simulation is further validated by analytical calculations using x-ray mass attenuation coefficient from:

<http://physics.nist.gov/PhysRefData/XrayMassCoef/ElemTab/z26.html>

The simulation confirms that 2 mm SS is sufficient for shielding the beam when scraping pipe at perpendicular incidence angle. Table 2.18 lists the simulation results along with the assumed beam intensity at 7 keV and at the third and fourth harmonics. The monochromatic beam intensity was calculated using the undulator spectrum and assuming a conservative 0.1% bandwidth.

Table 2.18: SST dose rate calculation after 2 mm SS beampipe

Energy (keV)	Photons/s before shielding	Mass Attenuation Coefficient μ_{en}/ρ (cm ² /g)	Attenuation factor: $\exp(-\mu_{en}/\rho * \rho * 2 \text{ mm SS})$	Photons/s after shielding	Dose rate*(mrem/h): 2mm SS shielding
7	10 ¹⁴	51.33	1.675E-35	< 0.001 photons/s	Negligible < 0.001 mrem/h
21	10 ⁵	22.6	4.881E-16	< 0.001 photons/s	
28	10 ³	7.251	1.223E-5	0.01 photons/s	

* Photon flux is assumed on a 1 cm² surface. Photon flux to dose rate conversion factor was referred from ICRP74:

Scenario 2: Beam scattering off inclined Si target inside a 100 mm diameter SS chamber of 3 mm wall thickness. Also simulate the same chamber with 6 mm and 12 mm glass.

Based on STAC8 calculation, 3 mm SS or 6 mm glass (SiO₂) is sufficient to shield scattered radiation from a Si target. The dose rate is calculated at 100 mm distance (<0.01 mrem/h).

Scenario 3: Beam hitting a SS flange beamstop to determine the beamstop thickness for the direct beam.

The dose rate after a 2 mm thick SS beam stop is small averaged on a 1 cm² area, as confirmed by simulations on scenario 1. From a health physics aspect, the dose effect over a 1 cm² area is considered reasonable for a small synchrotron beam. To be conservative, Amy Xia recommends using 1" thick SS flange as a direct beam stop.

Though SST does not intend to use glass view ports as beam stop, the dose rate from direct beam hitting a glass viewport was simulated and found to be not acceptable: The dose rate from direct beam hitting 6 mm SiO₂ glass is 1.37E+03 mrem/h; And the dose rate from direct beam hitting 12 mm SiO₂ glass is 1.13E+02 mrem/h. Thus, we will make sure that all the glass view ports are covered with leaded glass of equivalent to 0.25 mm Lead (attenuation equivalent to 2 mm Stainless Steel at 7 keV) where there is a possibility for direct beam to hit the view port.

3 Endstations

The SST endstations are made up of 6 unique NEXAFS/XPS experimental stations located within 55 to 70 meters of the center of the straight. Four of them are located on the soft branch and two on the tender, all with varying beam spot sizes. The two on the tender branch will have the ability to utilize the soft and tender X-rays sequentially or simultaneously. All experimental stations will operate under vacuum (hutchless) and are equipped with state-of-the-art detectors and analyzers with their associated electronics.

3.1 Discussion of endstations

XPS Microscope Station: This new XPS microscope, shown below in Fig. 3.1, has been under development at NSLS (U4A). It is an SBIR Phase-III collaboration between NIST and *R. Browning Consultants*. To date, 4 Patents have been granted for this new microscope technology. At NSLS-II it will receive soft and/or tender beams via two ellipsoidal mirrors that have a common focal spot of 13 μm . The new XPS microscope can be thought of as a superconducting magnetic projection lens x-ray photoemission electron microscope (XPEEM). The full field magnetic projection lens enables large depth of field nanoscale spatial and spectral XPS imaging over the full range of kinetic energy (100 eV to 7.5 keV) tuning the sensitivity from surface to bulk length scales ideally suited for photovoltaics and microelectronics. There are no high voltages; samples can be rough or insulating. Thus the XPS microscope, combines nanometer scale spatial resolution and depth selectivity with XPS chemical and electronic state specificity to enable full three-dimensional (3D) chemical mapping of the structure of nanomaterials and nanodevices at all points within their volume.

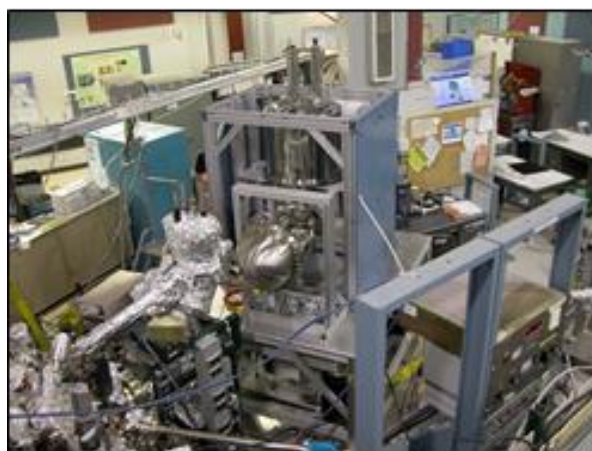


Fig 3.1: XPS microscopes shown at the U4A beamline of the NSLS.

Existing X24 HAXPES/ NEXAFS Station, pictured in Fig.3.2, will be the only undulator-based hard x-ray photoelectron spectroscopy (HAXPES) facility in the United States and is in high

demand by industry, for, example, microelectronics interfacial characterization (e.g., SEMATECH). This automated high-throughput station has a load lock system capable of holding up to 50 samples at a time and a High Energy Scientia 4000 electron analyzer. Additionally, for NEXAFS it has a large solid angle electron yield detector and a 7-element Ge ultra-high resolution x-ray detector for soft and tender x-ray fluorescence yield. This HAXPES/XPS/NEXAFS station has been transferred to NSLS-II where it will receive soft and tender x-rays (100 eV to 7.5 keV) at a common focal point of less than 100 μm with intensity to enable at least a 10x gain in sample throughput over operation at NSLS X24A and improved x-ray energy resolution using near normal incidence Si(333) crystals with the collimated undulator beam.

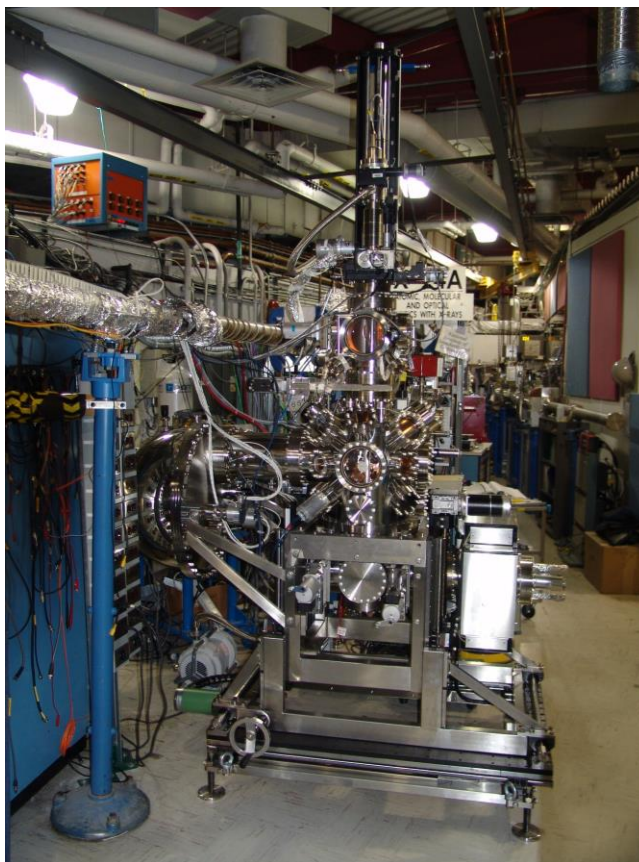


Fig 3.2: HAXES/NEXAFS beamline from the X24A beamline of the NSLS.

Existing U7A NEXAFS/XPS Station: The U7A NEXAFS/XPS station, shown in figure 3.3, was utilized 24/7 at the NSLS for OPVs, nanomaterials, biomaterials, batteries, polymers and polymer interfaces (see science case examples). This automated high-throughput station has a

load lock system capable of holding up to 100 samples at a time and a Scienta Wide Angle 4000 electron analyzer. For Electron Yield (EY) NEXAFS, it has a large solid angle CEM detector and a novel 36 channel detector array for measuring EY at all takeoff angles and at all angles of x-ray incidence simultaneously for high-throughput NEXAFS depth profiling of surface treatments in advanced materials. For Fluorescence Yield NEXAFS, it has a -CsI-coated CEM x-ray detector and a unique focusing graded multilayer mirror and proportional counter for ultra-low background FY NEXAFS; e.g., reaction intermediates in catalysts. This NEXAFS/XPS station has been transferred to NSLS-II where it will receive soft x rays (100-2200 eV) at a focal point of less than 100 μm with intensity to enable at least a 10x gain in sample throughput over operation at NSLS U7A. A dithering system will allow mm spot sizes when performing NEXAFS on radiation sensitive samples.



Fig 3.3: NEXAFS/XPS beamline from the U7A beamline of the NSLS.

Large Area Imaging NEXAFS Microscope Station, pictured schematically in figure 3.4, is a working prototype station transferred from NIST's U7A beamline. It is a highly efficient 1 Tesla magnetic projection partial-electron yield full-field microscope imaging 13x18 mm at 50 μm spatial resolution with a large depth of field (rotatable sample see figure 3.4). It also has a variable entrance grid bias for depth profiling and extraneous electron rejection as well as charge mitigation. The microscope has been used to image combinatorial arrays of SAMs, batteries, OPV and various designer surfaces (see science case examples). This automated high-throughput prototype NEXAFS imaging station has a load lock system capable of holding up to 10 samples at a time.

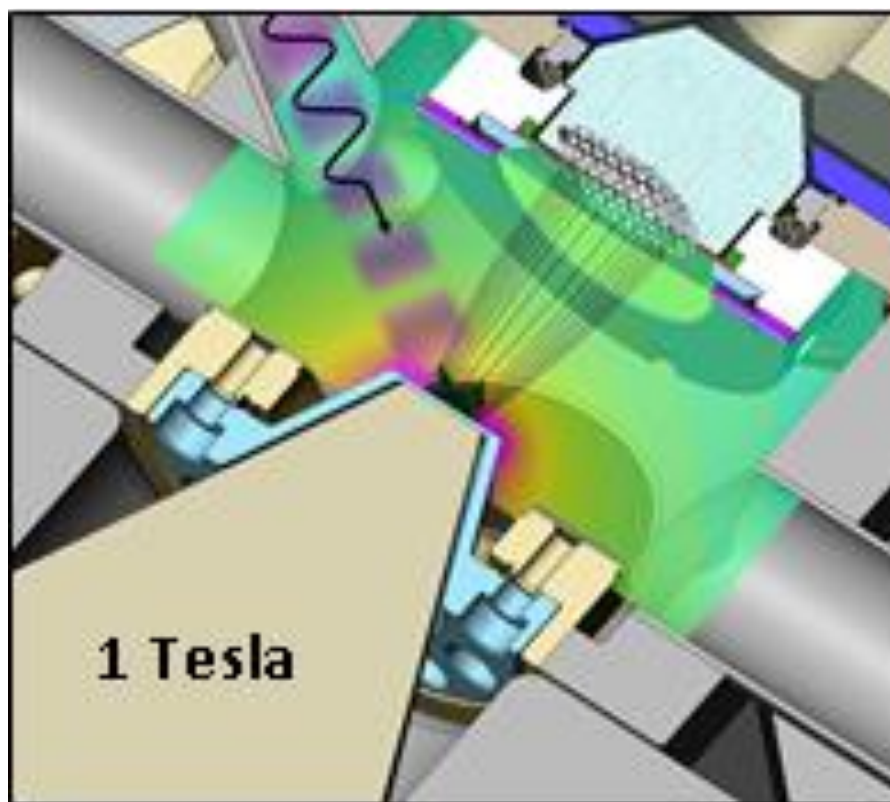


Fig 3.4: Schematic illustration of the large area imaging NEXAFS Microscope Station that was installed at the U7A beamline of the NSLS.

Large Area Imaging NEXAFS Microscope (MKII) Station is an ARRA funded (FY09 NIST SBIR Phase III with *Synchrotron Research, Inc.*) superconducting magnet (8T) NEXAFS microscope for NSLS-II that was developed at NSLS U8B beamline. The new superconducting microscope will produce highly efficient, highly parallel spectroscopic chemical and orientation maps of gradient samples, combinatorial arrays (e.g. 1000s of compositional samples at a time), and device arrays up to 4 cm^2 with simultaneous micron scale resolution. This microscope end

station has been transferred to NSLS-II and will receive soft x rays (100-2200 eV) from a pair of dithered mirrors providing 4x4 cm high flux sample illumination.

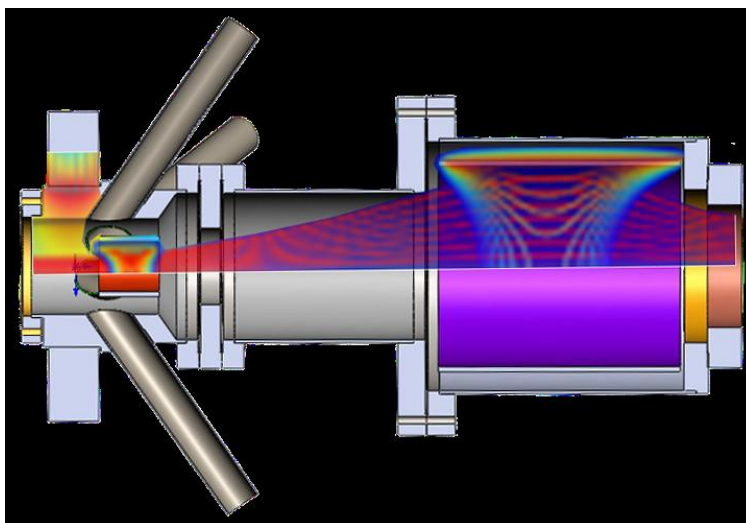


Fig 3.5: An illustration of the large area imaging NEXAFS Microscope (MKII) Station that was under development at U8B beamline of the NSLS

U7A High Pressure in-situ Soft X-ray NEXAFS and Emission Station pictured schematically in Fig.3.6 is a prototype station developed at NIST's U7A beamline and NIST in Boulder Colorado. NIST is pioneering a 10 mm² area, 256 element, micro-calorimeter soft x-ray detector that will be capable of better the 1 eV resolution at 25 kHz count rate for low background FY NEXAFS and soft x-ray-energy dispersive emission spectroscopy. This automated high-throughput station has a load lock system capable of holding up to 100 samples at a time. High pressure capability will be achieved with windows and cells that are in routine use in soft x-ray microscopy. This station has been transferred to NSLS-II where it will receive unfocused soft x rays (100-2200 eV) with spot size of 1 mm².

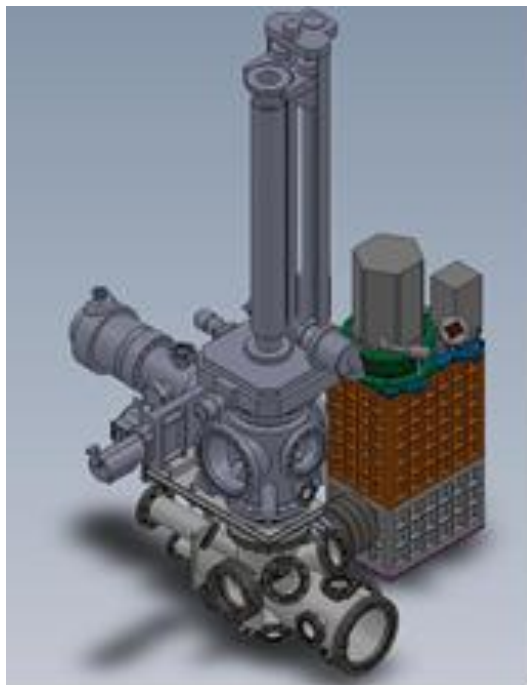


Fig 3.6: Schematic illustration of the high pressure in-situ soft x-ray NEXAFS and emission station prototyped at U7A beamline.

High Pressure in-situ Tender X-ray NEXAFS/XAS Station: The station, to be developed, will have FY and EY detectors, high pressure and *in-situ* operation to be achieved with standard windows and cells. *In-situ* catalytic studies of sulfide and chloride reaction intermediates will be routine in this station. At NSLS-II this end station will be located just downstream of the tender monochromator where it will receive unfocused tender x-rays (1-7.5 keV) with a spot size of 1 mm².

3.2 Beamline Utilities

The endstations will have the standard suite of utilities including electrical power, liquid and gaseous nitrogen, de-ionized (DI) water and process chilled water, compressed air and exhaust ventilation. The electrical requirement for SST is larger than most beamlines at the NSLS, and requires three transformers (50 kW each) instead of the usual two on the roof of the storage ring tunnel. The racks are designed to accept UPS power for the control circuits of motor drivers and other essential equipment. The utilities were distributed along the walls of the FOE, and via cable trays supported by pylons at the end-station area.

3.3 Equipment Protection System and Personnel Protection System

The Equipment Protection System (EPS) consists of sensors for 21 thermocouples (all in the FOE), 21 vacuum gauges (cold cathode gauge, 6 in FOE, 15 on the experimental floor), 30 ion pumps (8 in FOE and 22 on the experimental floor), and sensors and actuators for 27 gate valves, of which 6 are in the FOE and 21 are on the experimental floor. Fig. 3.7 shows the location of the vacuum sections (VS), gate valves (GV) ion pumps (IP). Water flow sensors on the experimental floor are also included in the EPS interlock

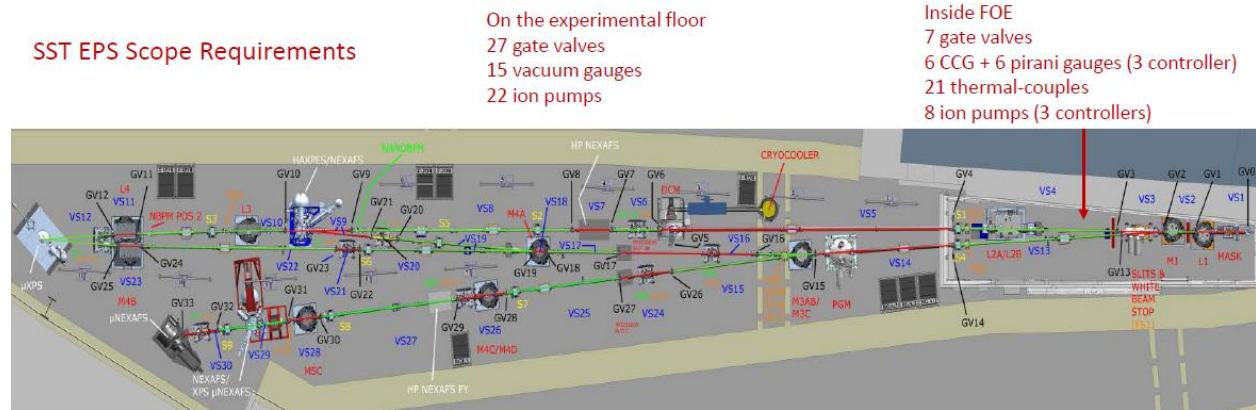


Fig 3.7: Markup showing locations of EPS components.

The personnel protection system (PPS) for the FOE will be based on standard NSLS-II FOE design. Fig. 3.8 shows the locations for the PPS components. The FOE PPS includes a set of redundant sensors and interlocks for the cooling water of the white-beam safety components (white-beam mask and stops), and a separate set of flow interlocks for the two pink-beam shutters. It also includes interlocks for PPS aperture, one labyrinth on the side wall facing the walkway, and the door switches and actuators, and all the shutter position switches.

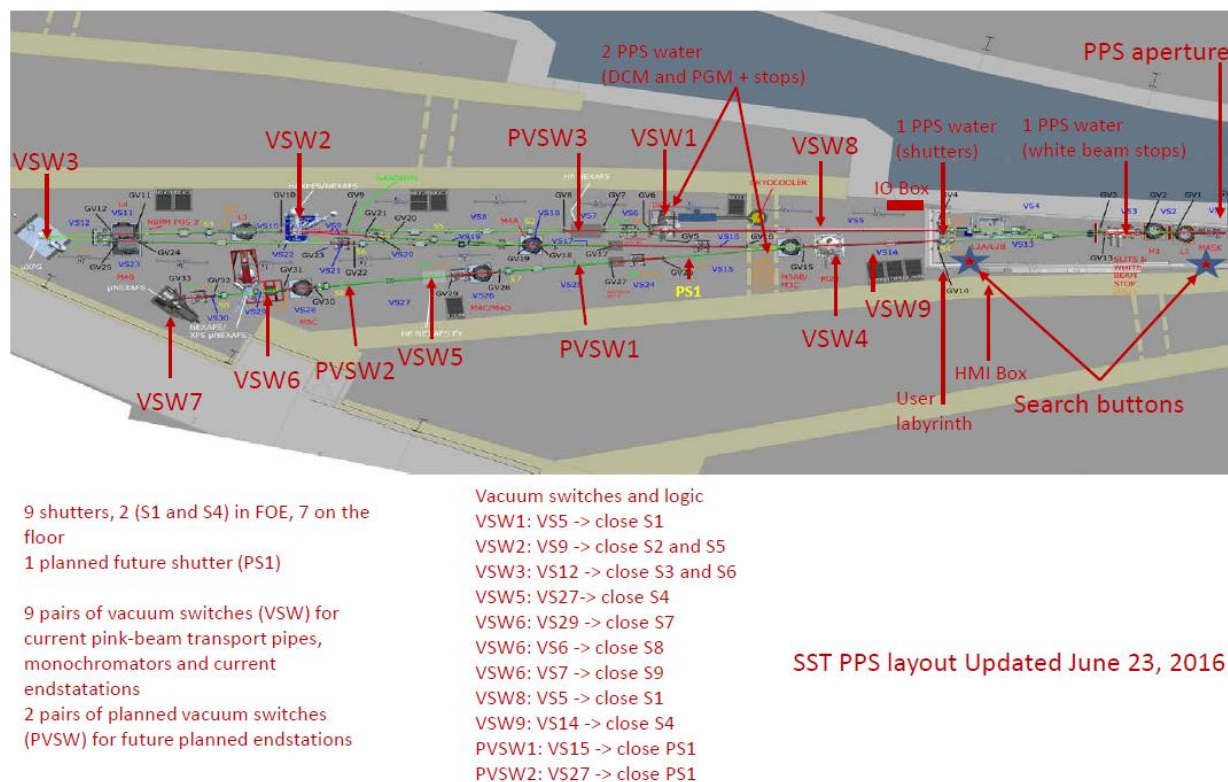


Fig 3.8: Markup showing locations of PPS components.

On the experimental floor, each endstation is designed to have its own shutter to allow access to its downstream endstation while the upstream endstation takes beam. The HAXPAS and micro-XPS endstations will each be served by two shutters since they receive beams from both the soft and tender branch. The beamlines will have 9 shutters in total.

SST PPS on the experimental floor adopts a design similar to that of CSX beamline developed by Stuart Wilkins and co-workers that incorporates PPS-rated redundant vacuum switches to prevent the shutters for the experimental endstations from opening when the endstation is vented. NSLS-II design policy requires vacuum switches for pink or white beam transport pipes on the experimental floor, monochromators and endstations regularly vented by users. As shown in Fig. 3.8, each endstation and monochromator chamber will be equipped with one pair of vacuum switches. In addition, each pink-beam transport pipe will have a pair of vacuum switches. Vacuum switches in the VGM and DCM monochromators on the experimental floor and in the pink-beam transport pipes prevent the FOE shutters from opening when the pink-beam transport pipes or monochromators are open to atmosphere. If an endstation is vented, the vacuum switches for that

endstation will prevent the shutter or shutters serving that endstation from opening. If the pink-beam transport pipes, monochromators are receiving beam as indicated by the FOE shutter being open, the vacuum sensors, if triggered, will close the FOE shutter and dump the storage ring beam if the shutter fails to close in 3 seconds. For an endstation, if the shutters immediately upstream of the endstation and in the FOE are open and the vacuum switches indicate that the endstation has been vented, the PPS will also close the shutter upstream of the endstation and dump the stored electron beam if the shutter fails to close in 3 seconds.

13 pairs of SIL-3 rated vacuum sensors will be purchased from SS Scientific. 7 pairs will be used for existing endstation chambers and planned future endstation. 2 pairs are for the PGM and DCM chambers. 2 pairs are for the pink-beam transport pipes. 2 pairs will serve as spares. Except for the spares, each pair of vacuum switches will be equipped with a manual isolation valve separating it from the vacuum vessel it protects. The manual valve allows for periodic interlock testing of the vacuum switches by allowing the switches to be vented to atmosphere without venting the associated chamber. In normal operations, the manual valve will be kept open by configuration control. In addition to the manual valve, the assembly also includes a pump out port and valve, as shown in Fig. 3.9.

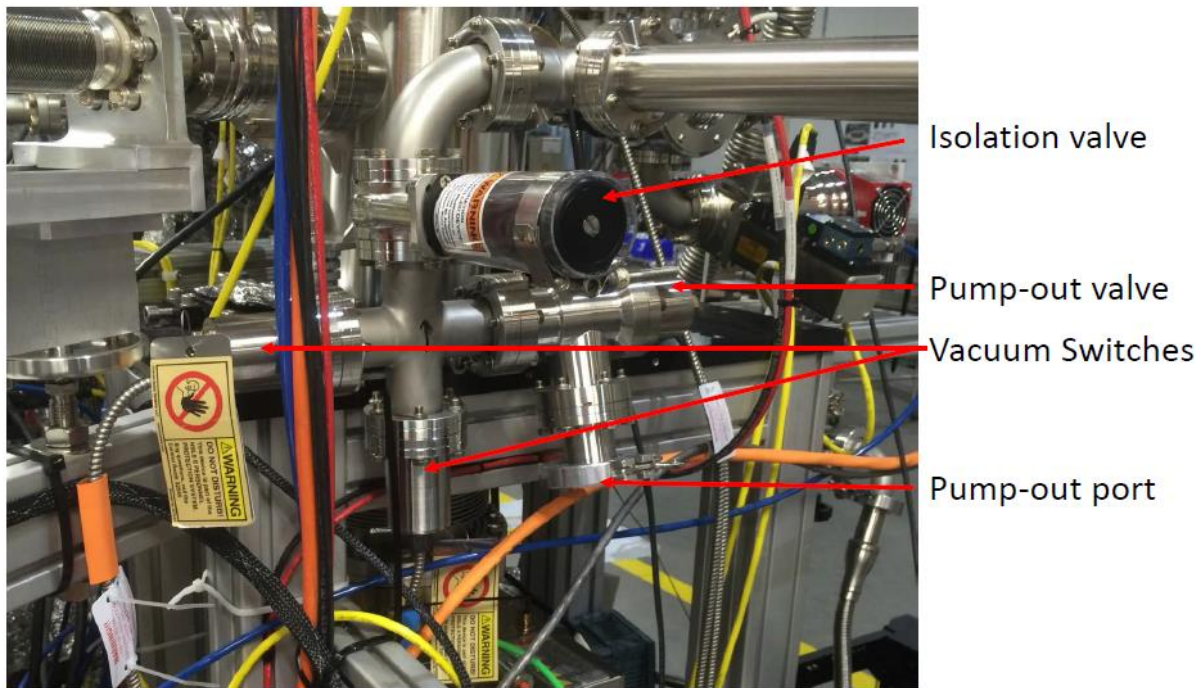


Figure 3.9: A typical vacuum switch assembly including isolation valve, redundant vacuum switches, and pump-out valve and port. The unit shown is installed at the CSX beamline.

As with the CSX and ESM beamlines, except for the endstation chambers, beam transport pipes, diagnostic modules, slit modules and mirror chambers at the monochromatic sections of the SST beamlines are not equipped with vacuum switches. Instead, users will be trained to not vent these vacuum sections. Beamline staff will be trained to vent these sections using established and approved procedures. The procedures will ensure that a beamline vacuum section is protected by at least one closed shutter and two closed gate valves upstream of the section before being vented.

3.4 Laboratory Space and Access

Laboratory space for the SST beamlines is located close to the beamlines in room 3LL04 which is shared by three other beamlines (IXS, SIX and ISR). Currently, we have space assigned in Lab6 of LOB3 for testing the EPU undulator. In the future, a laboratory dedicated to SST and BMM is desirable.

3.5 Work Area

The main control area for the SST will be downstream of the NIST sample prep cage which is downstream of the BMM work area and experimental hutch. A preliminary layout is shown in Figure 3.10. The arrangement facilitates sharing the setup cage with the BMM beamline, while maintaining independent control area for the SST and BMM beamlines.

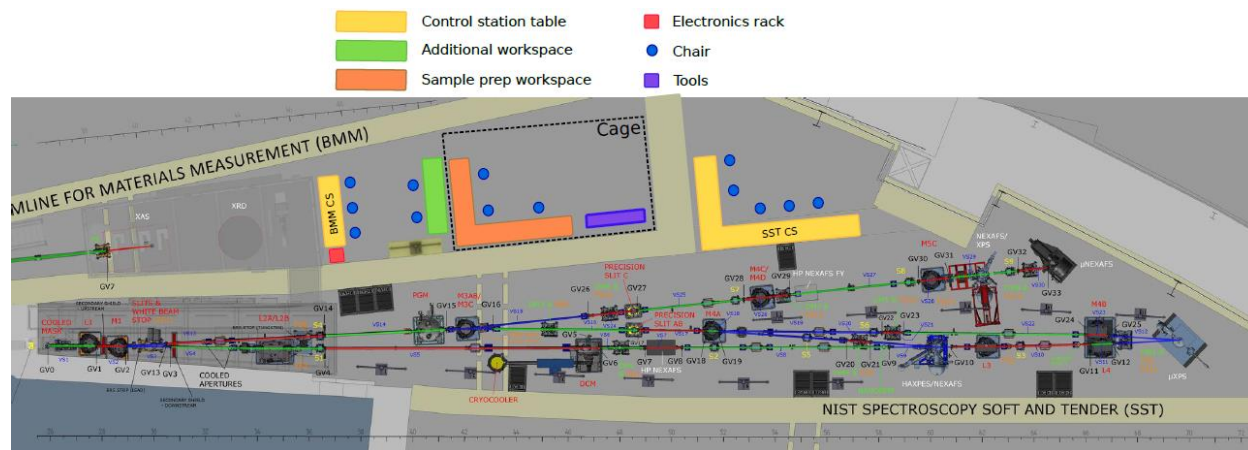


Figure 3.10: Work area for SST beamline, at the downstream of BMM beamline, and shared set-up space for BMM and SST.

4 Major Technical Risk Items

The requirements on the optics are achievable today. No new technical advances are required for delivering the proposed capabilities. Most of the endstations were in use till the NSLS shutdown in September 2014. We anticipate the following technical risks that are specific to the SST beamline:

4.1 Complexity of the beamlines

The SST1 and SST2 beamlines, with the unique feature of HAXPES/NEXAFS and μ XPS endstations being able to receive both soft and tender beams simultaneously, is likely to be the most complicated beamline at the NSLS-II and remain so for many years to come. The complexity was managed by generating detailed 3-D models of all the end stations before decommissioning from the NSLS, and by merging the 3-D models with the beamline design of FMB-Oxford to create the NSLS-II sector layout.

4.2 Relocation/Re-use of endstations

There is possibility of damage during equipment transfer of the endstations. The transferred endstations may not be compatible with NSLS-II standards in terms of safety, regulations, and software integration. All the transferred endstations will be evaluated for compatibility with NSLS-II safety regulations and software integration and any problematic issues discovered will be addressed using NSLS-II guidelines and lessons learned by earlier beamlines.

4.3 Operating hutch-less up to 7.5 keV

We will ask M. Benmerrouche to perform a detailed study of the shielding requirements for both monochromatic beam transport pipes and the endstations of both branches. Preliminary work by P. Berkvens (ESRF) and Amy Xia has shown this risk to be small and/or resolvable. Steel or lead shielding will be added to the transport pipes or endstations if the simulations show isolated, local weakness in shielding.

4.4 Repurposed Undulators from ESRF and Wisconsin

The EPU60 undulator was shipped to BNL in early 2015, and has been unpacked, checked for magnetic field hazard, and is currently being refurbished for controls by Johnny Kirkland. The refurbishment involves replacement of the encoders and motor connectors to conform to NSLS-II standards. The magnetic-field measurement will be made after the controls upgrade. The U42 undulator was received from ESRF in the summer of 2015, and has been unpacked and checked for magnetic field hazard. The U42 refurbishment will be performed after the EPU60.

4.5 Endstation Issues

Accidental Venting

All the endstations will be operated under UHV. To prevent/manage accidental venting, users will be fully trained on vacuum safety and the main venting sources (valves) will be properly sealed and will carry clear and easily visible warning labels/signs. In addition, fast trigger valves will be installed following NSLS-II guidelines on vacuum safety to mitigate any accidental venting.

Hazardous gas issues

Some of the endstations will use gases that may present ODH or other hazards but they will be handled appropriately to ensure safety first. The gas lines will be tightly sealed with safety valves installed to prevent continuous/accidental release. In addition, we will get NSLS-II ES&H staff to verify all handling procedures and safety of the gases as well as gas installations before they are used.

Different operating modes

As a multi-purpose, multi-branch, multi-endstation beamline, SST employs sophisticated operating modes that delivers the desired beam, of desired spectral and focal properties. In particular, choice of dither/non-dither, leads to different beam sizes along the beamline leading to the endstation. This poses technical risk for alignment and initial experimental setup changing endstations. The risk is mitigated by asking FMB-Oxford to perform a study to ensure that diagnostic screens are properly sized to capture all possible beam sizes. We also plan to develop a lookup table of motor positions for different operating modes during commissioning.

5 Safety

In addition to safety precautions related to the synchrotron source, the SST beamline will provide proper emergency egress routes and capability to handle samples and associated chemicals and gases appropriately.

The FOE and the experimental stations are located in a relatively enclosed area, thus care must be taken to guarantee adequate egress routes in case of emergency. Two egress routes are provided; one standard walkway with unimpeded access from the FOE and experimental stations to the outer walkway along the length of the beamline, and a duck-under path located upstream of the FOE door with access to the BMM egress routes.

There is concern that 7.5 keV x-rays from the tender branch may pose radiation risk at the endstations. A preliminary study of the scattered synchrotron radiation dose for the endstations and the monochromatic beam transport pipes downstream of the monochromator shows that the endstations comply with the NSLS-II radiation safety standards. Further studies of the monochromator tank before IRR, as well as radiation survey during commissioning serve to mitigate this risk. Furthermore, limits can be set on the monochromator to restrict the beamline to lower energy if needed.

Appendix A

Rubin Renninger's report for the optical design of SST.

p1

Appendix B

FMB Table of optics (location/specs).

p11

Appendix C

FMB PDR documents and review reports

p14

Appendix D

FMB FDR documents and review reports

p150

Appendix E

Preliminary Bremsstrahlung and synchrotron ray-tracing for SST beamlines

p 324

Appendix F

SST Beamline Development Proposal

p335